CONDITIONAL SIMULATION OF HYDROFACIES ARCHITECTURE: A TRANSITION PROBABILITY/MARKOV APPROACH[1]

STEVEN F. CARLE
Hydrologic Sciences, University of California, Davis, California 95616
Present address: Lawrence Livermore National Laboratory, L-206, Livermore, California 94551

ERIC M. LABOLLE, GARY S. WEISSMANN, AND DAVID VAN BROCKLIN
Hydrologic Sciences, University of California, Davis, California 95616

GRAHAM E. FOGG
Hydrologic Sciences and Dept. of Geology, University of California, Davis, California, 95616

ABSTRACT: In many hydrogeological investigations of groundwater flow and contaminant transport, considerable uncertainty arises from unknown physical heterogeneity of the aquifer system materials. Indicator geostatistics may offer tools for stochastic simulation of heterogeneity, however, existing methods were not designed with hydrogeological problems in mind. Typically, hydrogeological characterizations are vastly undersampled in lateral directions. Subsequently, geostatistical analyses must rely, in part, on geologic interpretation to yield geologically plausible results. Compared to traditional variogram-based approaches, the transition probability/Markov approach introduced herein more rigorously considers spatial cross-correlations (juxtapositional tendencies), yet is more conducive to integration of geologic interpretation. Three-dimensional (3-D) Markov chains are introduced as a conceptually simple yet theoretically powerful model of spatial variability, supported in theory and practice by numerous prior 1-D geologic applications to vertical sedimentary successions. The geostatistical conditional simulation algorithms of sequential indicator simulation and simulated quenching (zero-temperature annealing) are modified to include consideration for all spatial cross-correlations. "Non-stationarities" related to anisotropy directions, proportions of depositional units, and commingling depositional systems also can be considered. Example applications are given for alluvial fan and fluvial depositional systems in California in portions of the Livermore Valley, Kings River alluvial fan, and Salinas Valley.

[1] In, Fraser, G. S., and J. M. Davis, 1998, Hydrogeologic Models of Sedimentary Aquifers, Concepts in Hydrogeology and Environmental Geology No. 1, SEPM (Society for Sedimentary Geology) Special Publication, p. 147-170.

INTRODUCTION

Most researchers agree that realistic modeling of subsurface flow and transport processes requires realistic characterization of system heterogeneities. In particular, transport of fluids and solutes depends strongly on heterogeneity throughout a hierarchy of scales, many of which occur over distances shorter than typical borehole spacing. Difficulty in characterizing such unknown heterogeneity has been a major obstacle to accurate modeling of mass transport in both groundwater and petroleum systems. This difficulty is particularly acute in the lateral directions, where the subsurface typically is undersampled relative to the vertical. For this reason, some researchers (e.g. Anderson, 1989; Fogg, 1989; Phillips and Wilson, 1989; Tetzlaff and Harbaugh, 1989; Journel and Alabert, 1990; Deutsch and Journel, 1992; Koltermann and Gorelick, 1992; Davis et al., 1993; Scheibe and Freyberg, 1995; Webb and Anderson, 1996) have suggested incorporating geologic interpretation to estimate spatial variability. That is, instead of estimating the spatial variability of a hydrologic property, such as hydraulic conductivity (K), one focuses on characterizing the spatial variability of geologic facies. Then, the spatial distribution of geologic facies is simulated to provide a "template" for defining the spatial distribution of K. This approach presumes that a relationship between geologic facies and K can be estimated and that the spatial distribution of the geologic facies adequately represents the spatial distribution of K for purposes of modeling flow and transport processes.

A geologically sound template provides a scientific basis for modeling spatial variability of hydraulic properties. Clearly, subsurface patterns originate from geologic processes; hence, geology should be integral to subsurface characterization whether the approach is deterministic or stochastic. This includes geostatistical approaches, which should intensify, rather than minimize, the integration of geologic interpretation. If possible, the categories chosen for the template should have a geometric context, for example, depositional facies (channel bar, splay, flood plain) as opposed to purely textural descriptors (sand, silt, clay). Then, the interpretational framework of facies models can help guide the construction of geologically plausible hydrogeologic models.

The scale of interest in many hydrogeologic investigations often spans a large portion of a depositional system, for example, an alluvial fan or fluvial sedimentary sequence. At this regional or "aquifer system" scale, geometry and interconnectivity of, for example, fluvial channel and interchannel facies assemblages typically is more important to modeling groundwater flow than are smaller scale sedimentary structures such as cross-bedding. Thus, a model of the spatial distribution of larger scale facies with contrasting hydraulic properties, or "hydrofacies architecture," may be extremely useful as a model of hydraulic heterogeneity at the aquifer system scale.

Geostatistical methods have been applied to characterization of aquifer system heterogeneity, particularly for interpreting spatial variability of hydrofacies (e.g., Johnson and Dreiss, 1989; Wingle and Poeter, 1993; Johnson, 1995; Ritzi et al., 1995) and for conditionally simulating hydrofacies architecture (e.g., Wen and Kung, 1993; Ritzi et al., 1994; Poeter and McKenna, 1995, Bierkens, 1996). These applications have employed the "indicator variogram" to define spatial correlation structures (Deutsch and Journel, 1992). Indicator methods are appealing for hydrogeological numerical modeling applications because of the grid-based geometry, the consideration of conditioning data and the quantitative description of spatial variability. By enabling generation of multiple equiprobable "realizations," conditional simulation provides a means for assessing uncertainty and performing Monte Carlo analyses constrained by borehole data.

The geological community has been hesitant to accept geostatistical simulations of the subsurface, pointing out what they consider to be key shortcomings, such as the stationarity assumption and the inability to represent variable anisotropy directions, for example, radial morphology of an alluvial fan or meandering (Neton et al., 1994). Furthermore, sedimentary facies exhibit strong spatial cross-correlations (juxtapositional tendencies); for example, levee deposits tend to occur vertically and laterally adjacent to channel deposits. Clearly, a geologically plausible characterization of the subsurface ought to account for such juxtapositional relationships. Indeed, an essential aspect of geology is characterization of spatial arrangement of geologic units. Two questions about these geostatistical simulation approaches frequently arise:

1. How can one estimate a three-dimensional (3-D) model of spatial variability given that most geological data sets do not support direct calculation of the variogram in all directions?
2. Are indicator variogram statistics capable of adequately representing the natural configurations of heterogeneity found in the subsurface so that the "realizations" are, in fact, realistic?

This paper addresses both questions and provides an alter-

native geostatistical approach that facilitates development of models of spatial variability and produces greater geologic realism in conditional simulation results.

NEW GEOSTATISTICAL APPROACH

When a geologic system is modeled by categorizing several geologic units, some fundamental observable attributes are considered:

- volume fraction (proportions),
- lengths (e.g., thickness and lateral extent),
- juxtapositional tendencies,
- directions (e.g., orientation of bedding),
- nonstationarity (spatial trends) in the above.

A geostatistical method should attempt to capture these attributes. In addition, the practitioner needs tools to incorporate this fundamental information into a geostatistical characterization.

The need for a new geostatistical approach emerges in practical hydrogeological applications because existing geostatistical methods do not provide (1) consideration for asymmetric juxtapositional relationships such as fining-upward tendencies; (2) a conceptual framework for incorporating geologic interpretation of proportions, lengths and juxtapositional tendencies into development of cross-correlated spatial variability models; or (3) consideration for locally variable anisotropy directions, for example, radial morphology of alluvial fans, meandering of fluvial depositional units and structure resulting from deformation. Accordingly, these problems have inspired a new transition probability-based approach to indicator geostatistics that simplifies model development and interpretation (Carle and Fogg, 1996). Spatial variability is posed in terms of conditional probabilities of occurrence of the actual categories (geologic units, facies) rather than, for example, variograms of transformed variables such as cumu-latively-defined "discretization classes" (Gomez-Hernan-dez and Srivastava, 1990) or "principal components" (Suro-Perez and Journel, 1991). The transition probability approach is conducive to application of the mathematically simple yet theoretically powerful Markov chain models. Markov chain models can be developed not only by empirical curve-fitting approaches traditionally used in geostatistics but also by conceptual means through interpretation of proportions, mean lengths and juxtapositional tendencies (Carle and Fogg, 1997).

Geologists have long used transition probability measurements in conjunction with Markov chain models as tools for quantitative interpretation of vertical lithologic successions, starting with the pioneering work of Vistelius (1949) followed by many others including Carr et al. (1966), Vistelius (1967), Krumbein (1968), Krumbein and Dacey (1969), Schwarzacher (1969), Doveton (1971) and Miall (1973, 1982). Markov chain models also can be extended to 2-D and 3-D applications by assuming that 1-D Markov chains model spatial variability in any direction (Switzer, 1965; Lin and Harbaugh, 1984; Politis, 1994). A method for developing 2-D or 3-D Markov chains is presented, which enables creation of multi-category models of spatial variability with direction-dependencies in length (anisotropy) as well as juxtapositional relationships.

Although transition probabilities and Markov chains have long been applied in geology and statistics, their application to modern indicator geostatistical approaches is new. Markov chain models of spatial variability can be applied with minor modification to the geostatistical conditional simulation algorithms of sequential indicator simulation (SIS) and simulated quenching (zero-temperature annealing) described by Deutsch and Journel (1992, p. 123-125, 159-160). We find that a two-step of approach of initializing the simulation by SIS and then iteratively improving the simulation by simulated quenching produces better results than either algorithm applied by itself.

The new geostatistical approach has been developed in the context of hydrogeological applications, where data often are sparse yet three-dimensional (3-D) characterizations are needed. Three main steps are involved:

(a) evaluation of spatial variability of geologic units by transition probability measurements (if available) along principal stratigraphic directions of vertical (upward), dip and strike;
(b) development of Markov chain models of spatial variability by quantitative or conceptual means; and
(c) conditional simulation by successive application of the sequential indicator simulation (SIS) and simulated annealing algorithms.

The approach is applied to three Quaternary depositional systems in California (Fig. 1): (1) alluvial fan deposits at Lawrence Livermore National Laboratory (LLNL) in the Livermore Valley of the Coast Range, which contain a large proportion of fine-grained materials; (2) the Kings River alluvial fan in the eastern San Joaquin Valley southeast of Fresno, which contain extensive fluvial deposits; and (3) commingling alluvial fan and fluvial deposits in the Salinas Valley. In these applications we find that the conditional

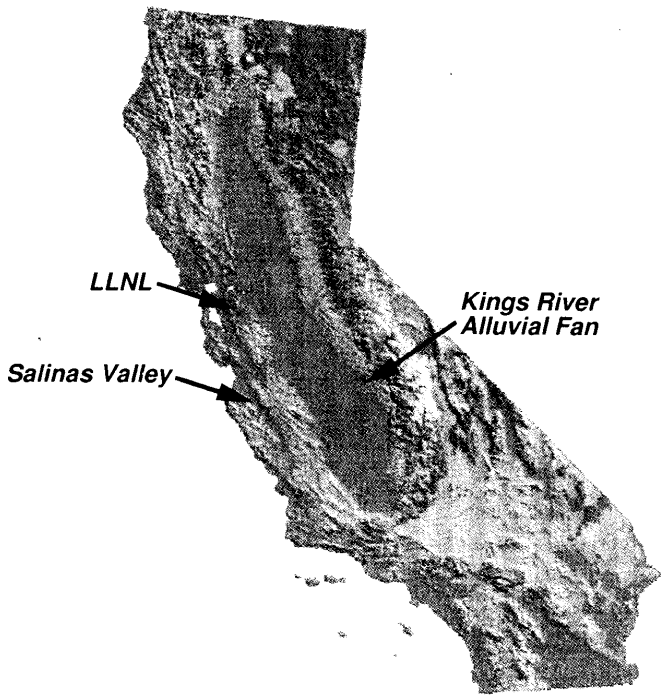

FIG. 1.– Map of California showing locations of Lawrence Livermore National Laboratory (LLNL), Kings River alluvial fan, and SalinasValley.

simulation results exhibit geologically plausible stratigraphic relationships consistent with available lithologic data.

TRANSITION PROBABILITY/MARKOV FRAMEWORK

In traditional geostatistical applications, the indicator variogram is incorporated as the measure of spatial variability for categorical variables, such as geologic units. Indicator variogram modeling procedures usually are empirical, involving fitting of mathematical functions to variogram measurements (Deutsch and Journel, 1992, p. 22-25). Alternatively, the transition probability can be used to describe spatial variability as well, particularly where asymmetries such as fining-upward tendencies are present (Carle and Fogg, 1996). Furthermore, the transition probability possesses interpretative advantages for relating fundamental properties of proportions, mean lengths and juxtapositional tendencies to parameters of the spatial variability model. These interpretive advantages are crucial to ensuring development of a geologically plausible model of spatial variability, particularly when data are too sparse to support a purely empirical approach.

In geostatistical conditional simulation applications, the transition probability can be used to formulate cokriging equations used for estimating local conditional probabilities in SIS and objective functions used in simulated annealing (Carle and Fogg, 1996; Carle, 1997). Thus, the transition probability can be used throughout the implementation of indicator geostatistical approaches, whether describing, modeling, or simulating the spatial variability of geologic units.

Definitions

In the application of indicator geostatistics, the indicator variable $I_k(\mathbf{x})$ defines the presence (or absence) of a category k (e.g., a geologic unit) at a location $\mathbf{x} \in \mathbf{D}$ by

$$I_k(\mathbf{x}) = \{ \begin{array}{l} 1, \text{ if } k \text{ occurs at } \mathbf{x} \\ 0, \text{ otherwise} \end{array} \qquad k = 1, ..., K \tag{1}$$

where K is the number of categories in a region $\mathbf{D}$ (e.g., a stratigraphic sequence). Assuming second-order stationarity, that is, the heterogeneity can be modeled throughout $\mathbf{D}$ by univariate (e.g., mean, proportions) and bivariate spatial statistics (e.g., indicator cross-variogram, indicator cross-covariance, joint probability, transition probability), the *model* of spatial variability will depend only on a separation vector or "lag" $\mathbf{h}$ and not on location $\mathbf{x}$. In geostatistics, indicator cross-variograms $\gamma_{jk}(\mathbf{h})$ and, more commonly, indicator variograms $\gamma_{kk}(\mathbf{h})$ (for $j = k$) as defined by

$$2\gamma_{jk}(\mathbf{h}) = E\left\{\left(I_j(\mathbf{x}) - I_j(\mathbf{x}+\mathbf{h})\right)\left(I_k(\mathbf{x}) - I_k(\mathbf{x}+\mathbf{h})\right)\right\} \tag{2}$$

traditionally are used to describe the spatial variability of indicator variables. Alternatively, the transition probability $t_{jk}(\mathbf{h})$ is simply defined according to a conditional probability:

$$t_{jk}(\mathbf{h}) = \Pr\left\{k \text{ occurs at } \mathbf{x}+\mathbf{h} \mid j \text{ occurs at } \mathbf{x}\right\}$$

$$= \frac{\Pr\left\{k \text{ occurs at } \mathbf{x}+\mathbf{h} \; and \; j \text{ occurs at } \mathbf{x}\right\}}{\Pr\left\{\, j \text{ occurs at } \mathbf{x}\right\}} \tag{3}$$

where

$$0 \le t_{jk}(\mathbf{h}) \le 1 \tag{4}$$

(Ross, 1993, p. 14). Applying (1) to (3), $t_{jk}(\mathbf{h})$ also can be

defined in terms of indicator variables as

$$t_{jk}(\mathbf{h}) = \frac{E\left\{I_j(\mathbf{x})I_k(\mathbf{x}+\mathbf{h})\right\}}{E\left\{I_j(\mathbf{x})\right\}} \tag{5}$$

Under the assumption of stationarity in $\mathbf{D}$, $E\left\{I_j(\mathbf{x})\right\}$ is equivalent to the volumetric proportions p_k of category k,

$$E\left\{I_k(\mathbf{x})\right\} = p_k \qquad \forall k \tag{6}$$

Applying (5) and (6) to (2), $\gamma_{jk}(\mathbf{h})$ relates to $t_{jk}(\mathbf{h})$ by

$$2\gamma_{jk}(\mathbf{h}) = p_j\left[2t_{jk}(0) - t_{jk}(\mathbf{h}) - t_{jk}(-\mathbf{h})\right] \tag{7}$$

(Carle and Fogg, 1996).

Thus, transition probabilities can be converted to indicator cross-variograms, if desired. Although indicator cross-variograms can be converted into transition probabilities in a similar manner, any information on asymmetry (e.g., a fining-upward tendency) would be lost from the outset because indicator cross-variograms assume symmetry by definition in (2). Additionally, existing indicator conditional simulation methods do not directly incorporate cross-correlation information because modeling of the full matrix of cross-covariances is considered tedious and impractical (Deutsch and Journel, 1992, p. 82, 149). Alternatively, indicator cokriging can be implemented with the transition probability (Carle and Fogg, 1996), inherently pointing to the Markov chain as a model of spatial variability for categorical (indicator) variables that fully considers cross-correlations (Carle and Fogg, 1997).

Continuous-Lag Markov Chains

Markov chain models applied to time series assume, in theory, that future occurrences depend on the present and not on the past. This simple stochastic model can address spatial applications by replacing the time lag with a spatial lag h_ϕ in a direction ϕ. The resulting mathematical expression of the continuous-lag formulation of a Markov chain model is

$$\mathbf{T}\left(h_\phi\right) = \exp\left[\mathbf{R}_\phi h_\phi\right] \tag{8}$$

(Krumbein, 1968; Agterberg, 1974, p. 457; Ross, 1993, p. 290), where $\mathbf{T}(h_\phi)$ denotes a $K \times K$ matrix of transition probabilities,

$$\mathbf{T}\left(h_\phi\right) = \begin{bmatrix} t_{11}\left(h_\phi\right) & \cdots & t_{1K}\left(h_\phi\right) \\ \vdots & \ddots & \vdots \\ t_{K1}\left(h_\phi\right) & \cdots & t_{KK}\left(h_\phi\right) \end{bmatrix}$$

and $\mathbf{R}_\phi$ denotes a $K \times K$ matrix of transition rates,

$$\mathbf{R}_\phi = \begin{bmatrix} r_{11,\phi} & \cdots & r_{1K,\phi} \\ \vdots & \ddots & \vdots \\ r_{K1,\phi} & \cdots & r_{KK,\phi} \end{bmatrix}$$

with entries $r_{jk,\phi}$ describing a conditional rate of change from category j to category k per unit length in the direction ϕ. By differentiation of (8) with respect to h_ϕ at $h_\phi = 0$, the transition rates are related to transition probabilities by

$$r_{jk,\phi} = \frac{\partial t_{jk}(0)}{\partial h_\phi} \tag{9}$$

(Ross, 1993, p. 290). Despite its theoretical simplicity, the Markov chain model has shown remarkable applicability to vertical lithological successions (Vistelius, 1949; Krumbein, 1968; Krumbein and Dacey, 1969; Schwarzacher, 1969; Harbaugh and Bonham-Carter, 1970; Doveton, 1994).

Comparison to Discrete-Lag Markov Chains

Geologic applications more commonly have employed the discrete-lag Markov chain, which is formulated from a transition probability matrix $\mathbf{T}(\Delta h_\phi)$ obtained from measurements at a discrete lag interval Δh_ϕ, usually chosen rather arbitrarily as a sampling interval. For the discrete-lag Markov chain model, $\mathbf{T}(n\Delta h_\phi)$ for $n = 0, 1, 2, ..., \infty$ is computed by successively applying the Chapman- Kolmogorov equation:

$$\begin{gathered} \mathbf{T}(0) = \mathbf{I} \\ \mathbf{T}(\Delta h_\phi) = \mathbf{I}\,\mathbf{T}(\Delta h_\phi) \\ \mathbf{T}(2\Delta h_\phi) = \mathbf{T}(\Delta h_\phi)\,\mathbf{T}(\Delta h_\phi) \\ \vdots \\ \mathbf{T}(n\Delta h_\phi) = \mathbf{T}\left[(n-1)\,\Delta h_\phi\right]\,\mathbf{T}(\Delta h_\phi) \end{gathered} \tag{10}$$

where $\mathbf{I}$ denotes the identity matrix (Agterberg, 1974, p. 420-421). However, any discrete-lag Markov chain model can be formulated as a continuous-lag Markov chain model

by applying (8) with $\mathbf{R}_\phi$ determined by

$$\mathbf{R}_\phi = \frac{\ln\left[\mathbf{T}\left(\Delta h_\phi\right)\right]}{\Delta h_\phi} \tag{11}$$

Advantages of the continuous approach are threefold. First, (8) represents the spatial variability model as a continuous function instead of discrete outputs only at fixed lag intervals as in (10). Second, the continuous-lag formulation of a Markov chain model is not dependent on issues of data spacing or sampling intervals because transition rates can be established by applying (11) to transition probabilities at any lag interval. Third, the ability to formulate the Markov chain as a continuous function enables the application to geostatistical simulation methods of SIS and simulated annealing.

Categorization – Facies Context

The first requirement toward applying the transition probability/Markov approach described is *categorization* or definition of the hydrofacies. In hydrogeologic applications at the aquifer system scale, categorization according to depositional facies is a desirable, if not mandatory, approach because it provides a scientific (geologic) basis for predicting geometry and spatial arrangement of hydraulic heterogeneity (Anderson, 1989; Anderson and Woessner, 1992, p. 29-37). At the LLNL site, comparison of well test results with detailed sedimentological analysis of core (Noyes, 1991) provide sufficient basis for establishing hydrofacies based on depositional facies. Admittedly, any facies-based categorization is only approximate. We would nevertheless argue that any attempt to place the subsurface characterization into a depositional facies context is an improvement over prevailing approaches in subsurface hydrology, such as the Unified Soil Classification System (Casagrande, 1948; ASTM, 1996) or Gaussian random fields, because it initiates and reinforces a geologically-informed characterization.

In many hydrogeologic applications, such as the Kings River fan and Salinas Valley sites, data consist primarily of descriptions of sediment textures, with little facies interpretation or hydraulic testing information. For the Kings River fan, facies interpretations were augmented by core samples, geophysics, soils surveys and analogy with modern systems. In the Salinas Valley case, the facies categories are only inferred from textural information. Regardless of data quality, the facies interpretation is needed to develop the three-dimensional geometric interpretive context that facies models provide (Miall, 1992). Nonetheless, the categorizations presented should be viewed as "operationally defined" to various stages of completion. This paper emphasizes the spatial variability modeling and conditional simulation of such characterizations rather than the methods used in facies interpretation.

TABLE 1.– BASIS FOR DEFINITION OF HYDROFACIES FROM LLNL CORE DATA.

#	facies	texture	%
1	*debris flow*	poorly-sorted clay-gravel	7
2	*flood plain*	clay and silt	56
3	*levee*	silty or clayey fine sand	19
4	*channel*	sand and gravel (rounded)	18

Application to LLNL – Vertical Direction

Groundwater contaminants, primarily volatile organic compounds, are present in alluvial fan deposits underlying LLNL (Fig. 1) over a regional extent of several km^2 to depths as great as 100 m (Thorpe et al., 1990). The aquifer system materials consist of a network of ancient stream channel and levee (including crevasse-splay) deposits and debris flows embedded in fine-grained flood plain deposits (Noyes, 1991). The lateral and vertical spatial extent of contaminants may be exacerbated by natural hydraulic interconnectivity of the subsurface channel/levee network (Carle, 1996). Working models of the hydrofacies architecture are needed to realistically assess contaminant fate and potential effectiveness of remediation efforts.

As summarized in Table 1, four hydrofacies were categorized as *debris flow*, *flood plain*, *levee* and *channel* facies based on detailed interpretations (Noyes, 1991) of portions of 5,500 m of core from vertical boreholes located near the southwest portion of LLNL and vicinity. The facies categorization was extended to the remainder of the core by interpretation of geophysical logs and textural descriptions noted by site geologists (Qualheim, 1988).

Figure 2 shows vertical (z)-direction transition probability measurements for the core data and a continuous-lag Markov chain model (8) developed by applying (11) to obtain a vertical transition rate matrix $\mathbf{R}_z$ for the $\mathbf{T}\left(\Delta h_z = 0.9 \text{ m}\right)$ measurement. The Markov chain model provides an excellent overall fit to the transition probability measurements, including the off-diagonal cross- correlations. As demonstrated by this four-category example, the Markov chain efficiently generates sixteen model structures $t_{jk}(h_z)$ from sixteen parameters $r_{jk,z}$ for $j, k = 1, ..., 4$.

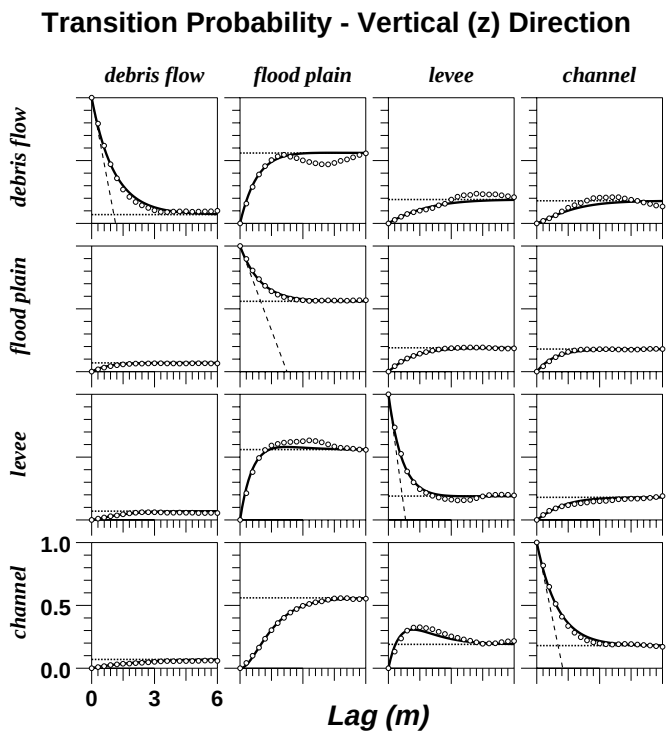

FIG. 2.– Matrix of vertical-direction transition probabilities for LLNL core data: measurements (dots) and Markov chain model (solid lines) obtained by applying equation (17) to the matrix of transition probability measurements at 0.9 m lag. Intersection of dashed line (tangent) with lag axis indicates mean length; dotted line indicates proportions.

Mathematically, the matrix exponential form of the Markov chain (8) is composed of linear combinations of exponential functions by (28), as described in the Appendix, where evaluation of the matrix logarithm (11) also is detailed. Nonetheless, a Markov chain can produce non-exponential-looking structures, for example, the "Gaussian"-like *channel →flood plain* and "hole-effect" *channel →levee* transition probability models in Figure 2.

MODEL CONCEPTUALIZATION

In the previous example the LLNL core data were relatively abundant for characterizing spatial variability of facies in the vertical direction and, thus, were conducive to application of the direct method of (11) to establish $\mathbf{R}_z$. However, spatial variability measurements may contain considerable uncertainty in lateral directions and, thus, may not be amenable to empirical modeling procedures. Only by understanding how model parameters relate to spatial variability can one address the important practical question, "Does this model make sense, geologically and probabilistically?" In practice, the parameters of a transition probability model can be directly related to fundamental interpretable properties of proportions, mean length, asymmetry and juxtapositional tendencies (Carle and Fogg, 1996; 1997).

Proportions

Assuming stationarity, the "sill" (asymptotic limit) of the transition probability is related to proportions by

$$\lim_{h_\phi \to \infty} t_{jk}(h_\phi) = p_k \qquad \forall j, k \tag{12}$$

If the proportions of the geologic units are known a priori, then (12) can be used to establish sills for the transition probability matrix. Conversely, the sill of the spatial variability model implies the assumed proportions. Equation (12) shows that the sills of each entry in the transition probability matrix will correspond to the proportions of the column category. For example, in Figure 2, the horizontal dotted lines indicate the sill of the vertical (z)-direction transition probability models for the kth (column) category in accordance with (12). As $h_z \to \infty$, the transition probability models clearly approach $p_1 \approx 0.07$, $p_2 \approx 0.56$, $p_3 \approx 0.19$ and $p_4 \approx 0.18$, corresponding to the percentages given in Table 1.

The point here is not to evaluate proportions from the transition probability sills, but rather to emphasize the straightforward relationship between proportions and the transition probability sill, which is useful for both data and model interpretation and, more importantly, for selection of plausible parameters for the model of spatial variability.

Mean Length

Although the "range" (the lag at which the sill is reached) commonly is used in geostatistics to describe spatial continuity and anisotropy, the "mean length" may function in a similar role. Let an "embedded occurrence" denote a distinct occurrence of a single category along a line in a particular direction, for example, a bed of gravel bounded by silt below and sand above. The mean length $\overline{L}_{k,\phi}$ of the category k in the direction ϕ is defined as the total length of category k along lines in the direction ϕ divided by the number of embedded occurrences of k along lines in the

direction ϕ. For example, the vertical (z)-direction mean length $\overline{L}_{k,z}$ would correspond to a "mean thickness." Thus, mean length represents a general term for "mean thickness" in any (stratigraphic) direction.

Mathematically, mean length $\overline{L}_{k,\phi}$ relates to a diagonal transition probability $t_{kk}(h_\phi)$ by

$$-\frac{\partial t_{kk}(0)}{\partial h_\phi} = \frac{1}{\overline{L}_{k,\phi}} \tag{13}$$

(Carle and Fogg, 1996). Application of (9) to (13) shows that a diagonal transition rate $r_{kk,\phi}$ directly relates to mean length by

$$r_{kk,\phi} = -\frac{1}{\overline{L}_{k,\phi}} \tag{14}$$

According to (13), the mean length will be indicated on a plot of the autotransition probability by the intersection of the tangent at the origin with the ordinate axis, as depicted by the dashed lines in the diagonal entries of Figure 2. Equation (13) can be used during model development either to establish the slope at the origin given knowledge or interpretations of mean length or, conversely, to interpret mean length implied by a diagonal transition probability model. Furthermore, (14) implies that knowledge or estimation of mean length can be used to establish diagonal transition rates for Markov chain models.

In the two-category ($K = 2$) case of a Markov chain, the mean length $\overline{L}_{k,\phi}$ in a direction ϕ relates to the corresponding "effective range" parameter of "$3a_\phi$" traditionally used in geostatistics for an exponential structure (Deutsch and Journel, 1992, p. 23) by

$$\overline{L}_{k,\phi} = \frac{a_\phi}{1 - p_k} \qquad k = 1, 2$$

In situations of three or more categories ($K \geq 3$), however, each entry of the Markov chain becomes a sum of two or more exponential structures, which may have complex coefficients. Thus, mean length provides a more direct parameter than the "range" for development of Markov chain models with three or more categories.

Asymmetry

The term "asymmetry" is used here to denote dependence of the bivariate statistics on whether the lag is positive or negative. An important distinction between $\gamma_{jk}(\mathbf{h})$ and $t_{jk}(\mathbf{h})$ evident in (7) is that $\gamma_{jk}(\mathbf{h})$ is intrinsically symmetric because $\gamma_{jk}(\mathbf{h}) = \gamma_{jk}(-\mathbf{h})$, whereas (3) allows for asymmetry or the possibility that $t_{jk}(\mathbf{h}) \neq t_{jk}(-\mathbf{h})$ or, equivalently, $p_j t_{jk}(\mathbf{h}) \neq p_k t_{kj}(\mathbf{h})$ for $j \neq k$. This is an important consideration for modeling spatial variability of stratigraphic units in fluvial deposits, where vertically asymmetric juxtapositional relationships occur as a result of fining-upward tendencies (e.g., Allen, 1970). In Figure 2, a *channel* $\rightarrow$*levee* ($4 \rightarrow 3$) fining-upward tendency is indicated because $p_4 t_{43}(h_z) \gg p_3 t_{34}(h_z)$ for small h_z.

If juxtapositional relationships are indeed symmetric between two categories j and k in a direction ϕ, then the relation

$$t_{jk}(h_\phi) = \left(\frac{p_k}{p_j}\right) t_{kj}(h_\phi) \tag{15}$$

holds, where h_ϕ is a lag in a direction ϕ. Differentiation of (15) with respect to h_ϕ at $h_\phi = 0$ and application of (9) yields the relation

$$r_{jk,\phi} = \left(\frac{p_k}{p_j}\right) r_{kj,\phi} \tag{16}$$

for symmetric juxtapositional relationships between categories j and k in a direction ϕ. Equations (15) and (16) are useful during interpretation for determining whether juxtapositional relationships are symmetric and in model development for establishing symmetrical juxtapositional tendencies in the transition probability or transition rate matrices, if desired.

Juxtapositional Tendencies

When developing either a geological or a geostatistical interpretation, one might want to evaluate the extent to which measured or modeled transition probabilities indicate preferential juxtapositional tendencies (e.g., levee deposits laterally or vertically adjacent to channel deposits) versus relatively disordered facies successions. Indeed, the main application of transition probability/Markov models by geologists has been to quantitatively analyze how juxtapositional tendencies compare relative to various states of disorder, either relative to conditional probabilities of embedded occurrences (Miall, 1973, 1982), entropy of transition frequencies (Hattori, 1976), independence of transition frequencies (Turk, 1979, 1982) and transition probabilities with respect to proportions (Carle and Fogg, 1996). These quantitative interpretational frameworks also can be posed with respect to transition rates for continuous-lag Markov chains (Carle, 1996; Carle and Fogg, 1997).

In practice, the interpretation of transition rates with respect to proportions may be the simplest to implement because it requires the fewest assumptions. In this interpretive framework, one considers occurrences of facies successions relative to volumetric proportions p_k, that is, whether an occurrence of k adjacent to j occurs greater or lesser than indicated by the proportions p_k. Consider that $t_{jj}(h_\phi)$ is the conditional probability of a unit j "transitioning" to itself over a lag h_ϕ, so that the conditional probability of transitioning to any other unit $\neq j$ is $[1 - t_{jj}(h_\phi)]$. If the transition probability $\widehat{t}_{jk}(h_\phi)$ for $k \neq j$ depends on proportions p_k, then

$$\widehat{t}_{jk}(h_\phi) = [1 - t_{jj}(h_\phi)] \frac{p_k}{1 - p_j} \qquad \text{for } k \neq j \quad (17)$$

Differentiating (17) by h_ϕ at $h_\phi = 0$ and applying (14) yields a corresponding transition rate $\widehat{r}_{jk,\phi}$ referenced with respect to category proportions:

$$\widehat{r}_{jk,\phi} = \frac{p_k}{\overline{L}_{j,\phi}(1 - p_j)} \qquad \text{for } k \neq j \qquad (18)$$

Thus, a measured or modeled transition rate $r_{jk,\phi}$ can be compared to $\widehat{r}_{jk,\phi}$ to judge whether k occurs adjacent to j in the direction ϕ to a lesser or greater degree relative to the proportion of k.

Application to LLNL – Strike Direction

Borehole data usually are insufficient to quantify spatial variability in lateral directions, not only because of typically sparse lateral spacing but also unknown variations in depositional dip and strike. Thus, the development of spatial variability models can obviously benefit from integration of geologic interpretation. Recognizing that a Markov chain analysis can be used as an interpretive tool then, conversely, geologic interpretation can be used to help establish geologically plausible transition rates.

For example, the transition rate matrix developed for the vertical (z)-direction model of the LLNL data (Fig. 2) viewed in strictly quantitative terms is:

$$\mathbf{R}_z = \begin{bmatrix} -0.875 & 0.706 & 0.104 & 0.064 \\ 0.088 & -0.447 & 0.150 & 0.209 \\ 0.024 & 1.080 & -1.227 & 0.123 \\ 0.040 & 0.000 & 0.766 & -0.806 \end{bmatrix} \text{m}^{-1}$$

Alternatively, one could apply the concepts of mean length (to the diagonal entries) and juxtapositional tendencies relative to proportions (to the off-diagonal entries) to obtain an equivalent, but more conceptual, expression of the transition rate matrix:

$$\mathbf{R}_z = \begin{bmatrix} -\frac{1}{\overline{L}=1.14} & 1.34\widehat{r} & 0.58\widehat{r} & 0.38\widehat{r} \\ 1.24\widehat{r} & -\frac{1}{\overline{L}=2.24} & 0.77\widehat{r} & 1.14\widehat{r} \\ 0.23\widehat{r} & 1.27\widehat{r} & -\frac{1}{\overline{L}=0.82} & 0.43\widehat{r} \\ 0.58\widehat{r} & 0.00\widehat{r} & 4.1\widehat{r} & -\frac{1}{\overline{L}=1.24} \end{bmatrix} \text{m}^{-1} \qquad (19)$$

where, for simplicity, subscript notation is dropped such that $\overline{L}$ denotes the mean length as defined in (14), and $\widehat{r}$ denotes a transition rate dependent on proportions by (18). Insights into mean length and juxtapositional tendencies obtained from outcrops, geophysical interpretation, or facies models could be used to establish geologically plausible diagonal and off-diagonal transition rates.

Some additional tools from the laws of probability can simplify the conceptual development of a transition rate matrix. The row sums of $\mathbf{R}_\phi$ must obey

$$\sum_{k=1}^{K} r_{jk,\phi} = 0 \qquad \forall j \qquad (20)$$

and the column sums must obey

$$\sum_{j=1}^{K} p_j r_{jk,\phi} = 0 \qquad \forall k \qquad (21)$$

(Ross, 1993, p. 273). Application of (20) and (21) eliminates the need to specify row and column entries in $\mathbf{R}_\phi$ involving one category β, herein referred to as the "background category." Conceptually the background may be viewed as the category that "fills in the space" not occupied by the other categories. Thus, for a four-category system, only $3 \times 3 = 9$ of the $4 \times 4 = 16$ entries in the transition rate matrix need direct specification; the remaining entries can be determined by (20) and (21) according to the laws of probability. In any application, however, the entries in the transition rate matrix, including row and column entries involving the background category, should obey

$$r_{jj,\phi} < 0 \qquad \forall j$$

$$0 \leq r_{jk,\phi} \leq -r_{jj,\phi} \qquad \forall j, k \neq j$$

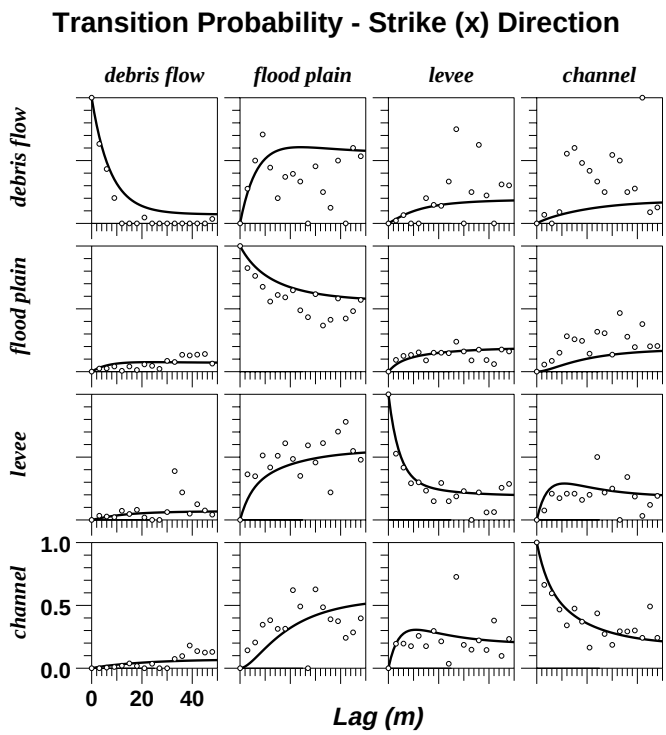

FIG. 3.– Matrix of strike-direction transition probabilities for LLNL core data: measurements (dots) and a Markov chain model (solid lines) based on conceptual interpretation of proportions, mean lengths, and juxtapositional tendencies.

and

$$0 \leq r_{jk,\phi} \leq -\left(\frac{p_k}{p_j}\right) r_{kk,\phi} \qquad \forall j, k \neq j$$

in order to satisfy (4).

In this example, *flood plain* (category 2) was chosen as background because, in general, it occupies space not occupied by other facies deposited by higher energy depositional processes. Mathematically, however, any category can be chosen as background. If symmetry of juxtapositional tendencies between two categories j and k in the direction ϕ is assumed, then relation (16) can be applied. For example, in the four-category case, if all juxtapositional relationships are assumed symmetric, then only *three* off-diagonal transition rates need to be specified once mean lengths, proportions and the background category are selected.

Strike (x)- and dip (y)-direction transition rate matrices $\mathbf{R}_x$ and $\mathbf{R}_y$ can be developed conceptually by applying estimates of mean length and proportions in conjunction with interpretation of lateral juxtapositional tendencies implied by Walther's Law, that a vertical facies succession corresponds to a lateral sequence of depositional environments (Leeder, 1982, p. 140). The mean lengths $\overline{L}_{k,x}$ for the strike direction can be established for the uncertain data in Figure 3 by considering plausible strike:vertical length ratios. Obviously, what constitutes a "plausible" mean length or elongation ratio is an interpretive matter that depends on the depositional system. Empirical geomorphic models of fluvial channel width:depth ratios (e.g., Etheridge and Schumm, 1978) could be used to guide the interpretation. In this example, assumed strike (x)-direction mean lengths of 8 m, 6 m and 10 m correspond to strike:vertical elongations ratios of 7.0:1, 7.4:1 and 8.1:1 for *debris flow*, *levee* and *channel*, respectively. The mean length for *flood plain*, the assumed background category, need not be specified. If the strike (x)-direction juxtapositional tendencies for *channel* →*levee*, *channel* → *debris flow* and *levee* →*debris flow* are assumed similar with respect to proportions as those for the vertical direction (19) in accordance with Walther's Law, the full strike- direction transition rate matrix $\mathbf{R}_x$ could be estimated by

$$\mathbf{R}_x = \begin{bmatrix} -\frac{1}{\overline{L}=8} & c_1 & s & s \\ c_2 & c_2 & c_2 & c_2 \\ 0.23\widehat{r} & c_1 & -\frac{1}{\overline{L}=6} & s \\ 0.58\widehat{r} & c_1 & 4.1\widehat{r} & -\frac{1}{\overline{L}=10} \end{bmatrix} \mathrm{m}^{-1}$$

where c_1 and c_2 denote successive application of (20) and (21) to respective row and column sums of $\mathbf{R}_x$, and s denotes an imposition of symmetric juxtapositional tendencies by applying (16). Note that only six of the sixteen entries in $\mathbf{R}_x$ need direct specification once proportions, symmetry and a background category are assumed. The solid lines in Figure 3 show the resulting strike-direction Markov chain model. A dip (y)-direction model could be developed in a similar manner.

Clearly, other interpretations could be made to estimate strike-direction transition rates for this model of facies architecture. These could be accomplished, for example, by tuning the off-diagonal transition rates to accommodate different preservation potentials for facies successions in different directions. Trial-and-error procedures also can be applied by generating stochastic simulations with an initial rate matrix, then adjusting the transition rates to obtain desired juxtapositional tendencies. The Markov chain framework, although simple in theory, provides considerable flexibility and versatility for modeling 1-D spatial variability.

MULTIDIMENSIONAL MARKOV CHAINS

2-D or 3-D Markov chain models can be developed by assuming that spatial variability in any direction can be characterized by a 1-D Markov chain (Switzer, 1965; Lin and Harbaugh, 1984; Politis, 1994). Although this may seem like a tenuous theoretical leap, the assumption here is merely that Markov chains might characterize spatial variability not only in the vertical but in other stratigraphic directions such as dip or strike. In a typical hydrogeological application, data coverage usually is inadequate to directly develop a 1-D Markov chain model for each of the infinity of directions. Alternatively, model development can focus on the principal directions, say the strike (x), dip (y) and vertical (z). Then 1-D Markov chain models for any direction can be interpolated from the principal direction models.

Considering that the transition probability matrix $\mathbf{T}(h_\phi)$ for an arbitrary direction ϕ depends entirely on $\mathbf{R}_\phi$, the interpolation of Markov chain models can be accomplished by ellipsoidally interpolating entries in the transition rate matrices for the principal x, y and z directions by

$$|r_{jk,\phi}| = \sqrt{\left(\frac{h_x}{h_\phi} r_{jk,x}\right)^2 + \left(\frac{h_y}{h_\phi} r_{jk,y}\right)^2 + \left(\frac{h_z}{h_\phi} r_{jk,z}\right)^2} \tag{22}$$

for all j and $k \neq \beta$, where h_x, h_y and h_z are the x, y and z direction components of $h_\phi = \sqrt{h_x^2 + h_y^2 + h_z^2}$. The remaining entries in $\mathbf{R}_\phi$ involving j or $k = \beta$ can be determined by applying (20) and (21). For the negative lag vector components, say h_{-x}, entries from the rate matrix $\mathbf{R}_{-x}$ corresponding to the opposite direction $-x$ are defined by

$$r_{jk,-x} = \left(\frac{p_k}{p_j}\right) r_{kj,x}$$

and used in (22) in place of entries for $\mathbf{R}_x$, in accordance with the backward Kolmogorov differential equation (Agterberg, 1974, p. 455-456). Figure 4 shows a two-dimensional transition probability model for the strike-vertical ($x - z$) plane as interpolated from the vertical (z)- and strike (x)-direction models previously developed and shown in Figures 2 and 3. The prescribed strike-direction symmetry is evident in that $t_{jk}(h_x, h_z) = t_{jk}(-h_x, h_z)$ for every entry. However, asymmetries are evident in the vertical direction, particularly for $t_{34}(h_x, h_z)$ and $t_{43}(h_x, h_z)$ because of a strong fining-upward tendency of *channel* →*levee*.

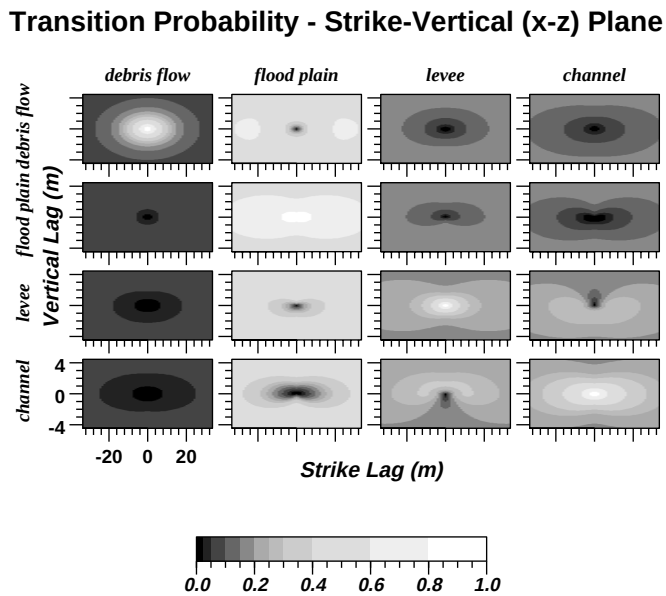

FIG. 4.– Two-dimensional Markov chain model for strike-vertical plane established by interpolating strike and vertical-direction 1-D Markov chain models.

CONDITIONAL SIMULATION

Considering that true subsurface heterogeneity or "the truth" cannot be exactly determined, conditional simulation algorithms attempt to produce multiple images that possess *patterns* of heterogeneity or "spatial variability" characteristic of the truth while honoring available data. The so-called "realizations" may be useful for implementing realistic models of groundwater flow and contaminant transport, uncertainty analyses, or Monte Carlo inversions.

The conditional simulation technique applied in this paper involves two steps: (1) establishment of an "initial configuration" by the sequential indicator simulation (SIS) algorithm (Deutsch and Journel, 1992, p. 123-125), and (2) iterative improvement of the SIS-generated initial configuration by the simulated quenching (zero-temperature annealing) algorithm (Deutsch and Journel, 1992, p. 159-160). The two steps are mutually dependent because SIS alone will not yield stochastic simulations that adequately honor the model of spatial variability, and quenching will not succeed without a rudimentary initial configuration (Carle, 1997). Both the SIS and quenching steps may rely on the same Markov chain model of spatial variability and, consequently, are conducive to implementation in succession.

Sequential Indicator Simulation

The initialization step follows the sequential indicator simulation (SIS) algorithm described by Deutsch and Journel (1992, p. 123-125, 148), except that a transition probability-based indicator cokriging estimate $[i_k(\mathbf{x}_0)]^*_{coK}$ is used to approximate the local conditional probabilities from data at N locations by

$$\Pr\{k \text{ occurs at } \mathbf{x}_0 \mid i_j(\mathbf{x}_\alpha);\ \alpha = 1, ..., N;\ j = 1, ..., K\}$$

$$\approx [i_k(\mathbf{x}_0)]^*_{coK} = \sum_{i=1}^{N}\sum_{j=1}^{K} i_j(\mathbf{x}_\alpha) w_{jk,\alpha} \qquad (23)$$

where $i_j(\mathbf{x}_\alpha)$ represents the value of an indicator variable at a location $\mathbf{x}_\alpha$ as defined in (1). The weighting coefficients $w_{jk,\alpha}$ are computed from a transition probability-based cokriging system of equations:

$$\begin{bmatrix} \mathbf{T}(\mathbf{x}_1 - \mathbf{x}_1) & \cdots & \mathbf{T}(\mathbf{x}_N - \mathbf{x}_1) \\ \vdots & \ddots & \vdots \\ \mathbf{T}(\mathbf{x}_1 - \mathbf{x}_N) & \cdots & \mathbf{T}(\mathbf{x}_N - \mathbf{x}_N) \end{bmatrix} \begin{bmatrix} \mathbf{W}_1 \\ \vdots \\ \mathbf{W}_N \end{bmatrix}$$

$$= \begin{bmatrix} \mathbf{T}(\mathbf{x}_0 - \mathbf{x}_1) \\ \vdots \\ \mathbf{T}(\mathbf{x}_0 - \mathbf{x}_N) \end{bmatrix} \qquad (24)$$

where

$$\mathbf{W}_i = \begin{bmatrix} w_{11,i} & \cdots & w_{1K,i} \\ \vdots & \ddots & \vdots \\ w_{K1,i} & \cdots & w_{KK,i} \end{bmatrix}$$

(Carle and Fogg, 1996). Using transition probability-based indicator cokriging instead of the traditional indicator kriging approach improves consideration of spatial cross- correlations in estimating local conditional probabilities for SIS. Figure 5 (top) shows the initial configuration state of a conditional simulation of strike-vertical architecture after applying the SIS algorithm using (23) and (24) with the strike-vertical 2-D Markov chain model shown in Figure 4. In Figure 6, vertical transition probabilities measured from this initial configuration seriously depart from the transition probability model, indicating that the SIS algorithm, by itself, does not generate a pattern of spatial variability consistent with the 2-D Markov chain model.

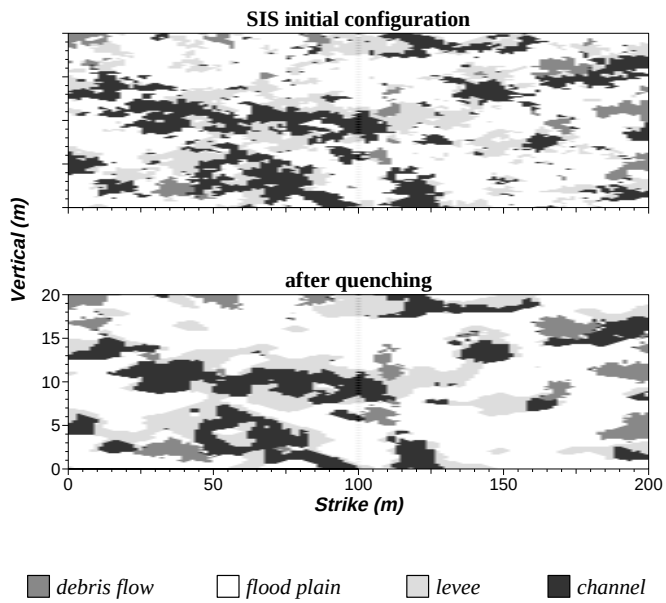

FIG. 5.– At top, SIS-based initial configuration of a 2-D conditional simulation of strike section hydrofacies architecture at LLNL. At bottom, final version of conditional simulation after implementing simulated quenching on initial configuration. Shaded center locations indicate conditioning data.

Simulated Quenching

The simulated quenching step is implemented to improve agreement between measured and modeled transition probabilities, starting from a SIS-generated initial configuration. The quenching step attempts to solve the optimization problem of

$$\min\left\{\mathbf{O} = \sum_{l=1}^{M}\sum_{j=1}^{K}\sum_{k=1}^{K} \left(t_{jk}(\mathbf{h}_l)_{MEAS} - t_{jk}(\mathbf{h}_l)_{MOD}\right)^2\right\} \qquad (25)$$

where $\mathbf{O}$ denotes an objective function, $\mathbf{h}_l$ denote $l = 1, ..., M$ specified lag vectors, and "$MEAS$" and "MOD" distinguish measured and modeled transition probabilities, respectively (Deutsch and Journel, 1992, p. 159-160). The simulated quenching algorithm is implemented by repeatedly cycling through each nodal location of the conditional simulation and inquiring whether a change to another category will reduce $\mathbf{O}$; if so, the change is accepted. This iterative improvement procedure continues until $\mathbf{O}$ is minimized, or a limit on the number of iterations is reached. Conditioning is maintained by not allowing changes of categories at conditioning locations. "Artifact discontinuity"

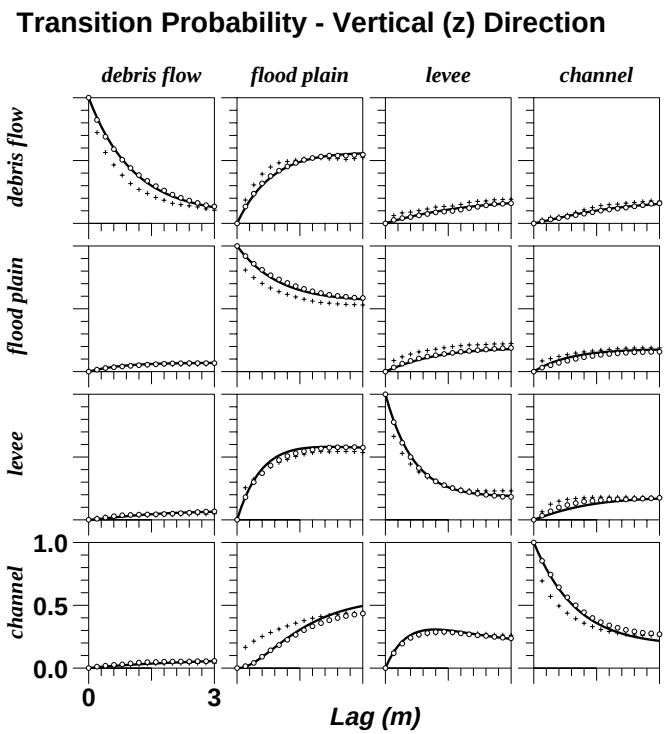

FIG. 6.– Comparison of the Markov chain model (solid lines) with vertical transition probabilities computed from SIS-generated initial configuration (crosses) and final conditional simulation in Figure 5 after applying simulated quenching (dots).

problems (Deutsch and Cockerham, 1994), where simulated patterns do not jibe with conditioning data, can be avoided by initializing the simulation with a SIS step instead of random values, choosing a minimal number of the closest lag vectors $\mathbf{h}_l$ for (25) and positioning the lag vectors in a configuration that considers the anisotropy of the spatial variability (Carle, 1997). Figure 5 (bottom) shows the result of applying simulated quenching to the SIS-generated initial configuration. After quenching, measured and modeled transition probabilities show excellent agreement (Fig. 6).

Note in Figure 5 that asymmetries of the fining-upward tendencies of *channel* $\rightarrow$*levee* are clearly apparent in the quenched conditional simulation. Such asymmetric juxtapositional relationships, which are strongly evident in the vertical transition probability measurements, cannot be simulated by traditional indicator variogram-based geostatistical methods.

Stationarity– Limitations and Possibilities

The stochastic methods described in this paper rely on an assumption of stationarity in the models of spatial variability. From the standpoint of geologic interpretation of alluvial fans, Neton et al. (1994) have criticized stochastic approaches for not considering directional variations, trends in lithofacies proportions and fan commingling. Granted, stationarity assumptions can constrain applicability of stochastic methods to limited regions. Nevertheless, it is possible to project nonstationary characteristics into the stochastic simulations, even though a stationary model of spatial variability is assumed. In the SIS step, conditioning data can enforce a nonstationarity in proportions, such as the coarsening-upward or fining-outward of an alluvial fan, through the "unbiasedness" property (consideration of *local* proportions) intrinsic to the transition probability-based indicator cokriging estimate. The quenching step generally preserves major features of the initial configuration, so that trends in proportions may persist to the end result of the conditional simulation (Carle, 1996). Nonstationarities in direction can be included in the conditional simulation if an a priori model of local directional variations is conceived, as shown in Figure 7 for the LLNL site, where seven parasequences associated with episodes of Quaternary alluvial fan deposition have been mapped (Blake et al., 1995). In this example, stratigraphic dip directions radiate from different source areas, such that anisotropy directions vary laterally and with depth corresponding to each depositional package.

If several depositional systems occur within a study region, different models of spatial variability can be ascribed to each depositional system. An example of this is given later in application to commingling braided-river and alluvial fan deposits in the Salinas River Valley. It also is possible to develop location-dependent spatial variability models.

KINGS RIVER ALLUVIAL FAN

The Kings River alluvial fan is located southeast of Fresno, where the Kings River enters the San Joaquin Valley at the western base of the Sierra Nevada (Fig. 1). Agricultural use of herbicides, pesticides and fertilizer has led to extensive non-point source contamination of the aquifer system (Nightingale, 1970; Kloos, 1983; Domagalski and Dubrovsky, 1991). Realistic models of hydrofacies architecture of the Kings River alluvial fan are needed to assess contaminant fate over a large regional extent.

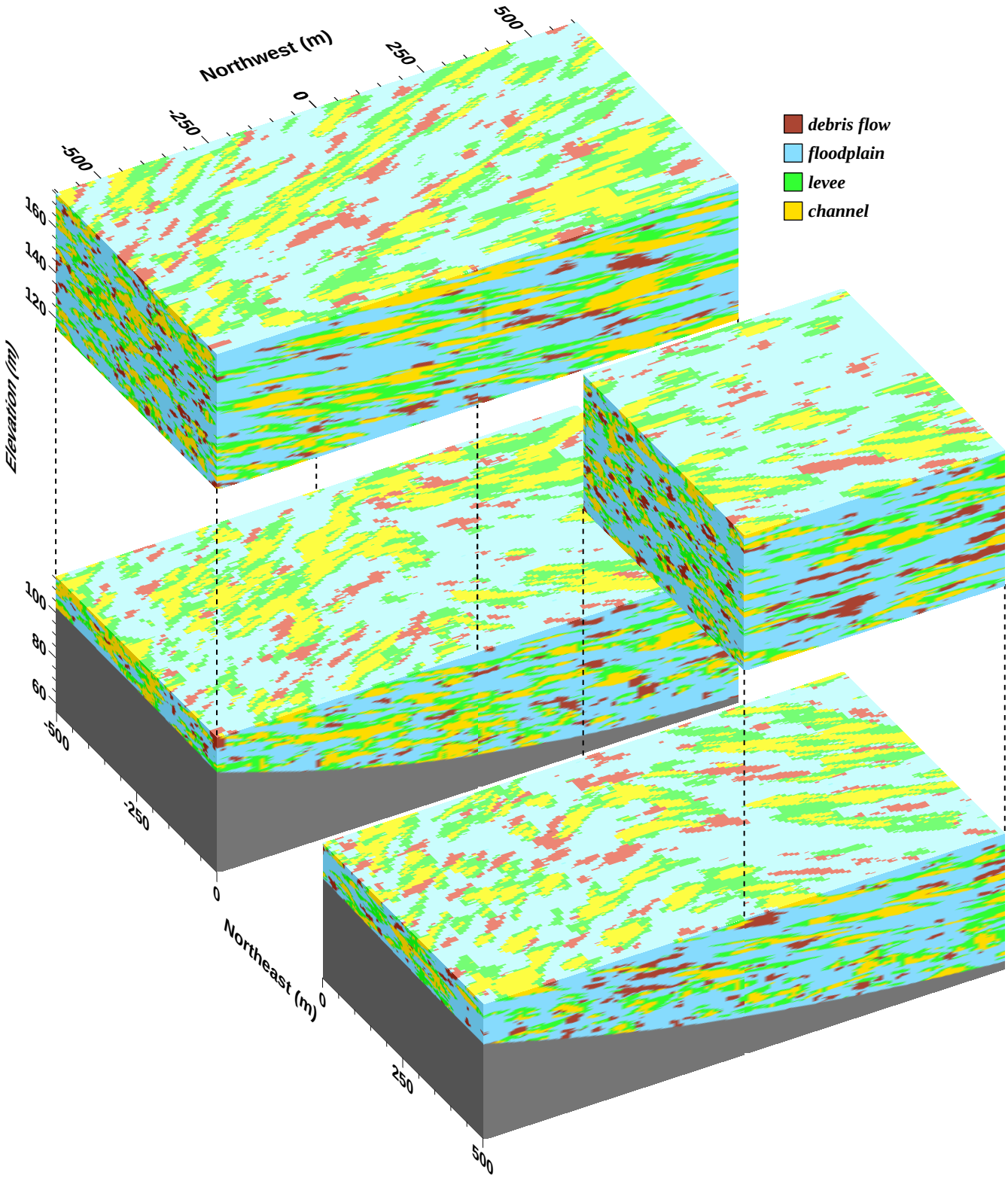

FIG. 7.– Threee-dimensional simulation of hydrofacies architecture at LLNL conditioned by 125 borehole logs on a $334 \times 120 \times 400$ node grid with a discretization of 3 m$\times$10 m$\times$0.3 m ($x \times y \times z$).

TABLE 2.– BASIS FOR DEFINITION OF HYDROFACIES FROM KINGS RIVER ALLUVIAL FAN CORE DATA.

#	facies	c-horizon texture	%
1	channel lag *gravel*	-	3
2	channel bar *sand*	sand, loamy sand	46
3	levee/bar *fine sand*	(fine) sandy loam	26
4	overbank *fines*	clay, silt, clay loam	25

In an effort to quantitatively characterize aquifer system heterogeneity, a detailed study area was established on a medial portion of the fan. Data available include 1:24,000-scale soil survey maps of c-horizon textures (U.S. Department of Agriculture, 1971), geophysical logs for seven test wells ranging in depth from 36 to 81 m, approximately 150 m of continuous core from three of the test wells, and 3.9 km of shallow seismic reflection and ground-penetrating radar (GPR) data. The core, logs and GPR and seismic data were obtained by the U.S Geological Survey in 1994 and 1995.

Geology

The Kings River alluvial fan deposits consist primarily of fluvially derived elongate gravel and sand bodies surrounded by overbank fine-grained material. Deposition primarily occurred during glacial episodes of the Sierra Nevada, with periods of nondeposition or erosion during the interglacials (Huntington, 1980). The fan sediments observed in the core and c-horizon (2 m depth) soil mapping were categorized into four hydrofacies based on sedimentalogical interpretations for the Kings River fluvial system (Table 2). Proportions of the hydrofacies are given according to the core data. Vertical juxtapositional relationships indicative of the fluvial setting, such as fining-upward tendencies (e.g., where *gravel* is overlain by *sand*, and *sand* is overlain by *fine sand*) were observed in the well data.

Sedimentologic categories similar to those seen in the core were recognized on the soil survey maps, as given by the c-horizon (2 m depth) textures shown in Table 2. Notably, *gravel* tends to be buried deeper than the 2-m depth of the soil samples; thus, corresponding soils generally are not evident on the map. The c-horizon map indicates relatively straight channel bodies, as well as lateral fining-outward (relative to channel axes) tendencies of *sand* →*fine sand* →*fines*. Compared to the core data, the proportions of fine-grained deposits are much greater in the c-horizon. Much of this difference probably relates to preservation potentials of the sediment types, where coarse-grained sediment tends to be preferentially preserved, and fine-grained material tends to be eroded and transported to distal portions of the fan.

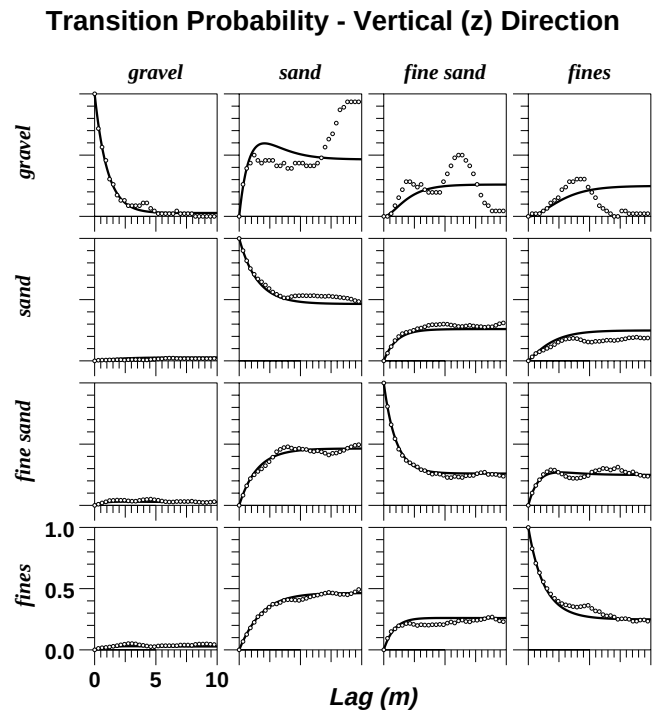

FIG. 8.– Matrix of vertical-direction transition probabilities for Kings River alluvial fan core data: measurements (dots) and Markov chain model (solid lines).

Markov Chain Modeling

Vertical (z)-direction transition probability measurements obtained from the core data, shown in Figure 8, were modeled by a Markov chain with a transition rate matrix of

$$\mathbf{R}_z = \begin{bmatrix} -\frac{1}{\overline{L}=1.06} & 2.10\widehat{r} & 0.00\widehat{r} & 0.00\widehat{r} \\ 0.57\widehat{r} & -\frac{1}{\overline{L}=2.73} & 1.44\widehat{r}_{23,z} & 0.59\widehat{r} \\ 1.64\widehat{r} & 0.68\widehat{r} & -\frac{1}{\overline{L}=1.33} & 1.53\widehat{r} \\ 1.69\widehat{r} & 0.67\widehat{r} & 1.51\widehat{r} & -\frac{1}{\overline{L}=1.70} \end{bmatrix} \mathrm{m}^{-1}$$

where the symbols are analogous to those in (19), $\overline{L}$ denoting mean lengths by (14) and $\widehat{r}$ denoting a transition rate relative to proportions by (18). Transition rates for the last row and column involving the background category (fines) were calculated by applying (20) and (21). Fining-upward tendencies are indicated by the transition rates of $2.10\widehat{r}$ and $1.44\widehat{r}$ for *gravel* →*sand* and *sand* →*fine sand*,

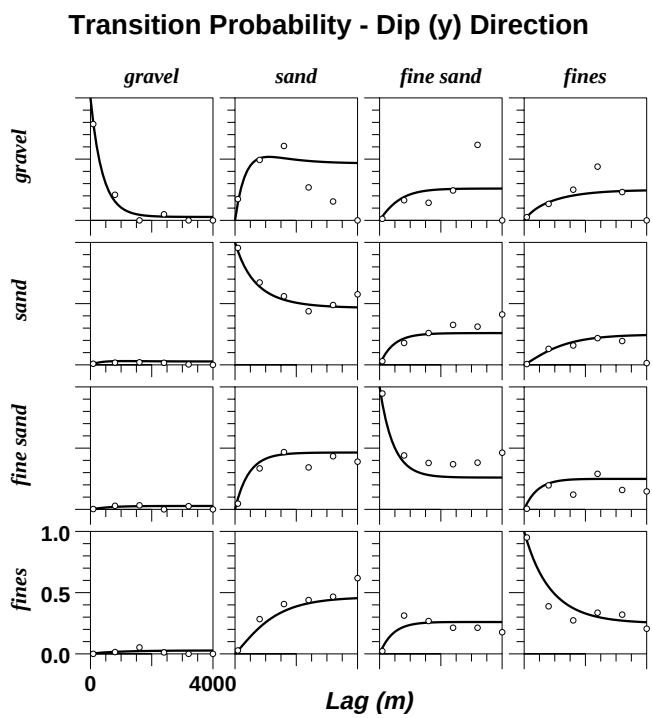

FIG. 9.– Matrix of dip-direction transition probabilities based on Kings River core data: measurements (dots) and Markov chain model (solid lines).

versus $0.57\widehat{r}$ and $0.68\widehat{r}$ for the opposing *sand* →*gravel* and *fine sand* →*sand* transitions. A tendency for *gravel* to occur as channel lag deposits beneath *sand* is strongly evident in the zero vertical transition rates for *gravel* →*fine sand* and *gravel* →*fines*. The relatively high transition rates of $1.53\widehat{r}$ for *fines* →*silty sand* and $1.51\widehat{r}$ for *silty sand* →*fines* indicate that *fines* and *silty sand* tend to be associated with each other. The relatively high transition rates of $1.64\widehat{r}$ for *silty sand* →*gravel* and $1.69\widehat{r}$ for *fines* →*gravel* indicate a tendency of the fluvial cycles to initialize in finer grained deposits.

The test wells were aligned in the general dip direction, which enabled an estimation of dip (y)-direction transition probabilities (Fig. 9), although considerable uncertainty results from the limited data and large well spacing. Markov chain modeling for the dip direction was facilitated by assuming the proportions given in Table 2, the overbank fines as the background category and symmetrical lateral juxtapositional relationships, as indicated by the soil survey. As a result, only six parameters needed to be specified for the dip-direction: mean lengths of the *gravel*, *sand* and *fine sand* categories and juxtapositional tendencies for *gravel* →*sand*, *sand* →*fine sand* and *gravel* →*fine sand*. Mean lengths of 400 m for *gravel*, 1,200 m for *sand* and 600 m for *fine sand* were assumed, which appeared consistent with spatial continuity indicated by the c-horizon maps and seismic and GPR surveys. The off-diagonal transition rates were tuned by trial-and-error to fit the data after first trying values measured from the soil survey and analogous to those applied to the vertical transition rates (a Walther's Law-style interpretation). The resulting dip (y)-direction transition rate matrix was prescribed by

$$\mathbf{R}_y = \begin{bmatrix} -\frac{1}{\overline{L}=400} & 1.50\widehat{r} & 0.55\widehat{r} & c_1 \\ s & -\frac{1}{\overline{L}=1200} & 1.44\widehat{r} & c_1 \\ s & s & -\frac{1}{\overline{L}=600} & c_1 \\ c_2 & c_2 & c_2 & c_2 \end{bmatrix} \mathrm{m}^{-1}$$

where s, c_1 and c_2 are prescribed by (16), (20) and (21), respectively.

Seismic and GPR data also indicated lateral continuity of fine-grained units for the strike (x) direction. Assumed mean lengths of 325 m for *sand* and 215 m for *fine sand* were checked for consistency with the soil map. A strike (x)-direction transition rate matrix was developed in a manner similar to the dip (y)-direction rate matrix by

$$\mathbf{R}_x = \begin{bmatrix} -\frac{1}{\overline{L}=150} & 1.50\widehat{r} & 0.55\widehat{r} & c_1 \\ s & -\frac{1}{\overline{L}=325} & 1.44\widehat{r} & c_1 \\ s & s & -\frac{1}{\overline{L}=215} & c_1 \\ c_2 & c_2 & c_2 & c_2 \end{bmatrix} \mathrm{m}^{-1}$$

The resulting transition dip (y)- and strike (x)-direction transition rate matrices yielded fining-outward tendencies that are, in general, less strict than the fining-upward tendencies of the vertical transition rates. This interpretation allows for the possibility that *gravel* may occur laterally adjacent to all categories, although primarily adjacent to *sand*.

Conditional Simulation

The conditional simulation of a portion of the Kings River alluvial fan shown in Figure 10 was generated on a $51 \times 51 \times 301$-node grid with a discretization of 50 m $\times$ 100 m $\times$ 0.3048 m ($x \times y \times z$). Conditioning was maintained by treating both the core data and facies interpretations of the geophysical logs as hard data. The simulation shows juxtapositional relationships that are consistent with a conceptual geologic model of the Kings River system. The *gravel*

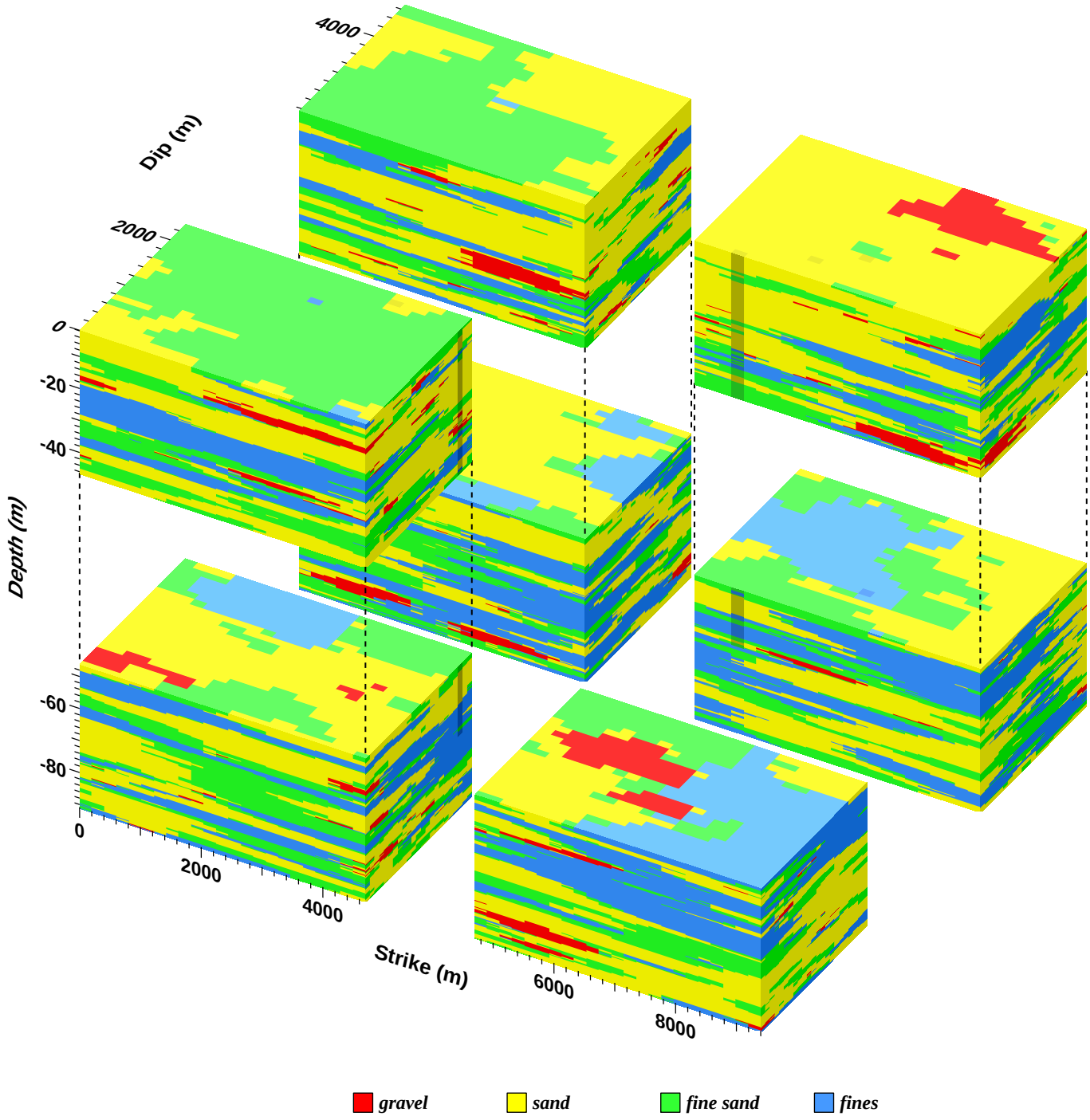

FIG. 10.– Conditional simulation of hydrofacies architecture in a portion of Kings River alluvial fan. Conditioning data (shaded) consist of core and geophysical logs from seven boreholes.

and *sand* categories tend to be strongly associated as elongate channel deposits with strong fining-upward tendencies of *gravel* →*sand* and *sand* →*fine sand*, as expected for a fluvial depositional system. The *fine sand* and *fines* categories tend to be associated with each other, as would be expected for upper channel, levee and overbank facies.

SALINAS VALLEY

In the Salinas Valley, elevated levels of nitrate in ground water are the result of historical land uses, which include irrigated agriculture, feed lots and on-site sewage disposal. Determining the impacts of such land-use practices on groundwater quality requires careful analysis of nitrate transport from land surface to water table. In turn, the impact of physical heterogeneity in the vadose zone is crucial to development of realistic nitrate transport models. A detailed study area was established at Wing Ranch, about 15 km southeast of Salinas (Fig. 1), in an effort to stochastically characterize three-dimensional vadose zone heterogeneity using the geostatistical methods described herein. Interestingly, the vadose zone at Wing Ranch consists of alluvial deposits from two depositional systems. This section describes an approach to including such a "nonstationarity" into geostatistical simulation.

Geology

The vadose zone at the Wing Ranch study area consists of fluvial deposits of the Salinas River and alluvial fan deposits originating from granitic Salinian basement terrains in the Gabilan Range to the northeast (Durham, 1974; Tinsley, 1975). Coarse-grained material from the Salinas River deposits can be distinguished from the alluvial fan deposits by the presence of Tertiary marine shale and chert derived from Monterey Formation rocks in the Sierra de Salinas southwest of Salinas Valley.

Seven boreholes were drilled to a depth of approximately 30 m. Cores were obtained continuously and categorized according to provenance and texture (Maserjian, 1993) as:

Salinas River deposits:	alluvial fan deposits:
1. *sand* (53%)	1. *sand* (43%)
2. *silty sand* (47%)	2. *silty sand* (46%)
	3. *fines* (11%)

where the percentages indicate the proportions of the textures observed in each depositional system. Based on lithologies observed in the study area, the alluvial fan deposits generally overlap the Salinas River deposits, although some interfingering of the depositional systems occurs.

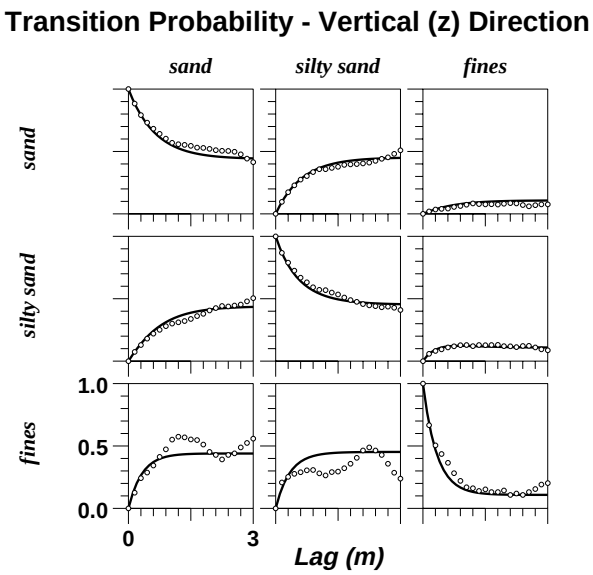

FIG. 11.– Matrix of vertical-direction transition probabilities based on core data for Salinas River deposits at Wing Ranch study area: measurements (dots) and Markov chain model (solid lines).

Markov Chain Modeling

The local patterns of heterogeneity in the Salinas River and alluvial fan deposits were assumed to be independent of each other. Vertical (z)-direction transition rate matrices for the two depositional systems were developed by fitting the vertical-direction transition probability measurements (Figs. 11 and 12) obtained from the core data, yielding

$$\mathbf{R}_{z,\text{SALINAS}} = \begin{bmatrix} -\frac{1}{\overline{L}=2.95} & c_1 \\ c_2 & c_2 \end{bmatrix} \text{m}^{-1}$$

and

$$\mathbf{R}_{z,\text{ALLUVIAL}} = \begin{bmatrix} -\frac{1}{\overline{L}=1.15} & 1.04\widehat{r} & c_1 \\ 0.63\widehat{r} & -\frac{1}{\overline{L}=0.98} & c_1 \\ c_2 & c_2 & c_2 \end{bmatrix} \text{m}^{-1}$$

where background categories were assumed as *silty sand* for the Salinas River system and *fines* for the alluvial fan system; diagonal transition rates are defined according to the mean length $\overline{L}$ as in (14); c_1 and c_2 denote application of (20) and (21), respectively; and $\widehat{r}$ denotes a transition

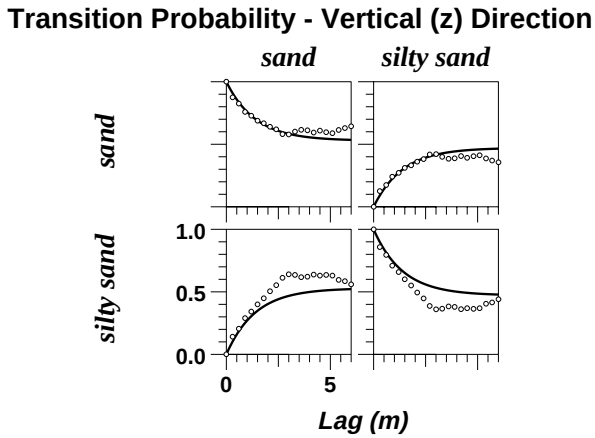

FIG. 12.– Matrix of vertical transition probability measurements based on core data for alluvial fan deposits at Wing Ranch study area: measurements (dots) and Markov chain model (solid lines).

rate dependent on proportions by (18). Note that no off-diagonal transition rates need to be specified in the two-category Salinas River case.

The lateral spacing of the boreholes is too large to establish a 3-D model of spatial variability directly from the data. Alternatively, transition rate matrices for the strike (x) and dip (y) directions were established interpretatively by assuming:

1. proportions, as given previously,
2. mean lengths corresponding to geologically plausible elongation ratios,
3. similar juxtapositional tendencies of *sand* →*silty sand* (1→2) as observed in the vertical, and
4. symmetric juxtapositional relationships in the strike (x) and (y) directions.

As a result, strike (x)- and dip (y)-direction transition rate matrices were obtained by

$$\mathbf{R}_{x,\text{SALINAS}} = \begin{bmatrix} -\frac{1}{\overline{L}=50} & c_1 \\ c_2 & c_2 \end{bmatrix} \text{m}^{-1}$$

$$\mathbf{R}_{y,\text{SALINAS}} = \begin{bmatrix} -\frac{1}{\overline{L}=200} & c_1 \\ c_2 & c_2 \end{bmatrix} \text{m}^{-1}$$

$$R_{x,\text{ALLUVIAL}} = \begin{bmatrix} -\frac{1}{\overline{L}=10} & 1.04\widehat{r} & c_1 \\ s & -\frac{1}{\overline{L}=8} & c_1 \\ c_2 & c_2 & c_2 \end{bmatrix} \text{m}^{-1}$$

$$R_{y,\text{ALLUVIAL}} = \begin{bmatrix} -\frac{1}{\overline{L}=40} & 1.04\widehat{r} & c_1 \\ s & -\frac{1}{\overline{L}=30} & c_1 \\ c_2 & c_2 & c_2 \end{bmatrix} \text{m}^{-1}$$

where s denotes application of (16), and c_1 and c_2 denote application of (20) and (21).

Conditional Simulation

A conditional simulation of hydrostratigraphy underlying the Wing Ranch study area (Fig. 13) was generated on a $101 \times 101 \times 101$-node grid with a discretization of 15 m $\times$ 15 m $\times$ 0.3 m ($x \times y \times z$). The simulation was produced in a similar manner as given in previous examples, except that another simulation step was added to distinguish the two depositional systems. First, conditional simulations of each depositional system were generated independently, as if only one depositional system existed in the vadose zone. Then, an additional conditional simulation was generated having two categories representing the two depositional systems. Using the proportions of the two systems, conditioning data and large assumed mean lengths, a geologically reasonable interface between the fluvial and alluvial fan systems was produced by a conditional simulation, which was then used to splice together the two independent conditional simulations of the Salinas River and alluvial fan hydrofacies architecture.

Nonstationarities in anisotropy directions also were considered. Meandering features were assimilated into the Salinas River deposits by assuming that anisotropy directions vary in the horizontal plane according to a Gaussian random field (Deutsch and Journel, 1992, p. 136-137). Stratigraphic dip directions of the alluvial fan deposits were fixed according to a radial morphology. The simulation illustrates two "nonstationarities" that can be incorporated in the geostatistical simulation of hydrostratigraphy: (1) nonstationarity attributed to different patterns of heterogeneity in each of two interfingering depositional systems, and (2) nonstationarity in anisotropy directions attributed to morphological features, such as meandering or radial alluvial fan morphology. These nonstationarities obviously would impact field-scale transport of nitrates. Conditional simulations such as this have been used for field-scale models of flow and transport to estimate contaminant arrival times from the land surface to the water table (Fogg et al., 1995).

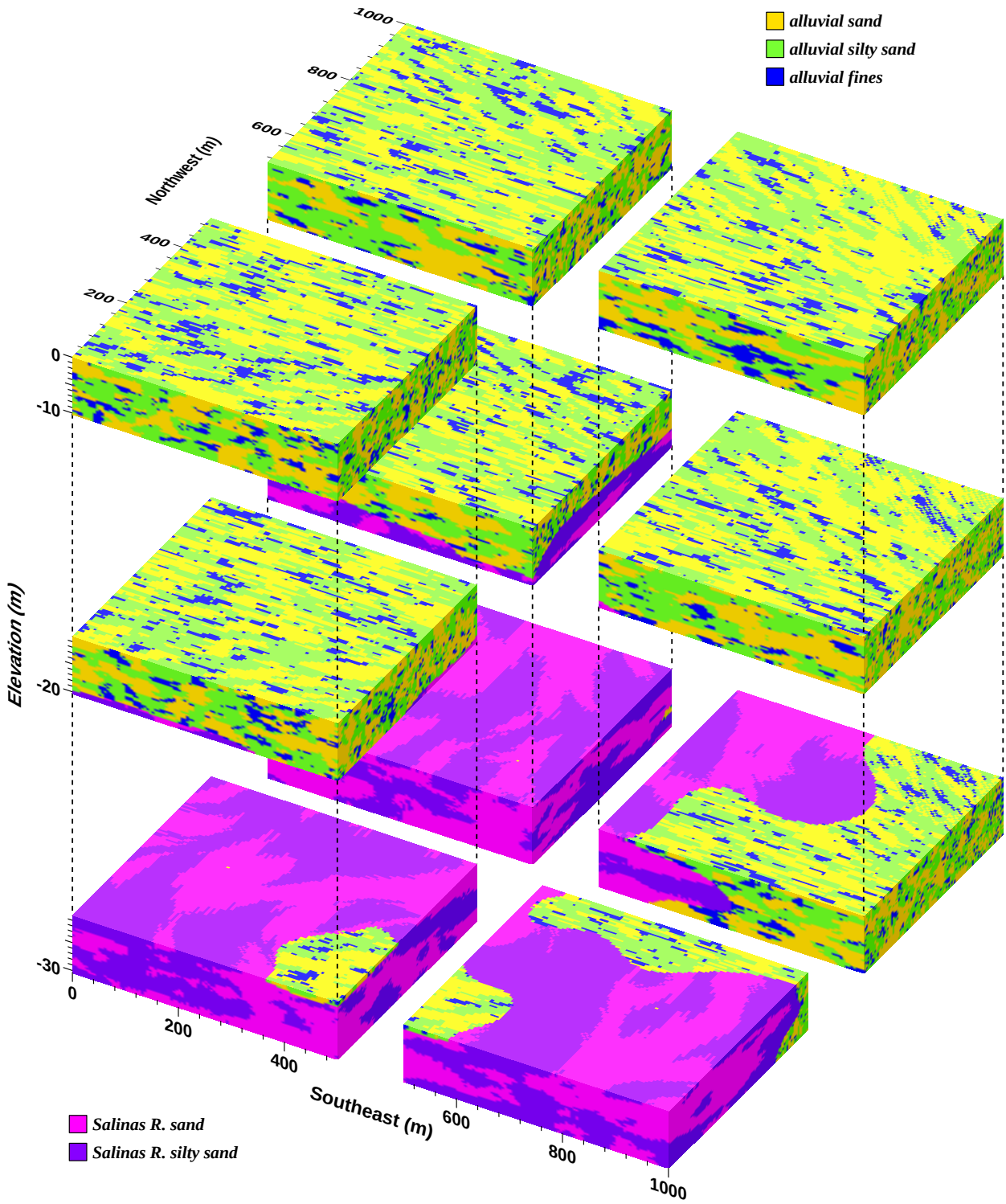

FIG. 13.– Conditional simulation of hydrofacies architecture at Wing Ranch study area, Salinas Valley, incorporating commingling alluvial fan and Salinas River deposits. Conditioning data consist of core descriptions from seven boreholes.

SUMMARY AND CONCLUSIONS

A new transition probability-based geostatistical approach to conditional simulation has been presented with example applications to alluvial and fluvial hydrofacies architecture. The approach improves the ability to incorporate geologic interpretation into geostatistical methods of conditional simulation, which is crucial for hydrogeological applications. Hydrogeological data typically are too sparse in lateral directions to apply the traditional geostatistical approach of empirical curve-fitting to variogram measurements. Furthermore, existing geostatistical approaches do not fully account for all spatial cross- correlations and, thus, cannot account for certain juxtapositional relationships such as fining-upward tendencies, which commonly occur in alluvial depositional systems.

The foundation of the approach is quantitative description of spatial variability of categorical variables (hydrofacies) in terms of the transition probability. The transition probability offers advantages over the more prevalent "indicator variogram" where integration of indirect, subjective, or conceptual information is desired. By simple graphical observation, features of the transition probability can be related precisely to geological attributes of proportions, mean length and juxtapositional tendencies. Such interpretability not only improves understanding of spatial variability measurements, but facilitates construction of geologically plausible spatial variability models.

The adoption of the transition probability as a measure of spatial variability points to employment of the Markov chain as a mathematically and conceptually simple yet theoretically powerful model of spatial variability. Markov chains have a long-standing track record in geology for quantitative analysis of vertical stratigraphic sequences. In the examples given, Markov chains consistently provide excellent models for measured vertical-direction transition probabilities of hydrofacies categories at three sites of alluvial and fluvial deposits in California.

Markov chain models can be extended to 3-D applications by modeling spatial variability in principal stratigraphic directions of vertical, strike and dip using either quantitative or conceptual means, then interpolating those 1-D models to all directions. Traditional geostatistical approaches rely on abundant data or an exhaustive "reference image" to empirically obtain a model of spatial variability. Alternatively, the Markov chain approach provides a conceptual framework for developing models of spatial variability through integration of fundamental information on proportions, mean length and juxtapositional tendencies. This approach is particularly useful in lateral directions, where data are typically sparse relative to the vertical. Sylvester's theorem (see Appendix) provides the mathematical foundations for calculating transition rate matrices and transition probabilities of 3-D, continuous-lag Markov chain models.

The 3-D Markov chain models of spatial variability then can be applied to both sequential indicator simulation (SIS) and simulated annealing geostatistical conditional simulation algorithms. In our experience, excellent conditional simulation results can be obtained by first applying SIS to generate an "initial configuration," then iteratively improving the SIS result by simulated quenching (zero-temperature annealing). As applied to fluvial deposits, the conditional simulations display geologically plausible juxtapositional tendencies. For example, at Lawrence Livermore National Laboratory, levee deposits tend to occur above and laterally adjacent to channel deposits; in channel bodies of the Kings River alluvial fan, gravel lag deposits tend to occur at the base of sand deposits. These fining-upward tendencies are strongly supported by core data but could not be properly simulated by prevalent indicator kriging-based SIS approaches. It is also possible to incorporate "nonstationarities" into the stochastic simulation results, even though models of spatial variability fundamentally assume stationarity. Nonstationarities in direction, such as meandering or the radial morphology of an alluvial fan, can be incorporated in the SIS and simulated quenching algorithms with an a priori map (deterministic or stochastic) of anisotropy directions.

In the techniques and examples given, we have emphasized integration of geologic interpretation into geostatistical methods. Granted, any geostatistical approach can be applied from a purely quantitative standpoint, such that categories defined according to "levee" or "channel lag" or "overbank fines" would assume no geologic significance. However, such geologic facies have geometric and locational significance in geologic interpretation, providing insight to characterizing true hydraulic heterogeneity patterns that otherwise would be difficult to characterize solely by statistics derived from typical hydrogeological data sets. Thus, we have attempted to present a geostatistical modeling approach that not only maximally utilizes univariate (proportions) and bivariate (transition probability) spatial statistics, but also brings out the "geo" aspect of "geostatistics."

APPENDIX: MATHEMATICAL FOUNDATIONS

In order to develop continuous-lag Markov chains as geo-

statistical models of spatial variability, one must be able to perform the following:

- evaluate the *matrix exponential* form of Markov chain given by (8),
- evaluate the *matrix logarithm* of a transition probability matrix given by (11), and
- convert a discrete-lag Markov chain to a continuous-lag Markov chain by combining (8) and (11).

However, (8) and (11) cannot be computed directly from the matrix entries. In either case, the key step is to find the eigenvalues of $\mathbf{R}_\phi$ or $\mathbf{T}(h_\phi)$, which can be computed using codes for real general matrices given by Smith et al. (1976) or Press et al. (1992).

For notational simplicity, let the lag $h = h_\phi$ and $\mathbf{R} = \mathbf{R}_\phi$. A square $(K \times K)$ matrix such as $\mathbf{R}$ can be expressed in diagonal form with respect to its eigenvalues by

$$\mathbf{R} = \sum_{l=1}^{K} \lambda_l \mathbf{Z}_l \tag{26}$$

where the λ_l for $l = 1, ..., K$ denote the eigenvalues of $\mathbf{R}$, and $\mathbf{Z}_l$ denotes a spectral component matrix associated with each eigenvalue λ_l. The spectral component matrices $\mathbf{Z}_l$ can be determined directly from the eigenvalues and matrix $\mathbf{R}$ by

$$\mathbf{Z}_l = \frac{\prod\limits_{m \neq l} (\lambda_m \mathbf{I} - \mathbf{R})}{\prod\limits_{m \neq l} (\lambda_m - \lambda_l)} \qquad l = 1, ..., K \tag{27}$$

where $\mathbf{I}$ denotes the identity matrix. The continuous-lag Markov chain (8) then can be computed from

$$\mathbf{T}(h) = \sum_{l=1}^{K} \exp(\lambda_l h) \mathbf{Z}_l \tag{28}$$

through application of Sylvester's theorem (Agterberg, 1974, p. 406-412). Recognizing that (28) represents a canonical form of $\mathbf{T}(h)$, two useful conclusions can be drawn for the Markov chain model:

1. The eigenvalues $\theta_l(h)$ of $\mathbf{T}(h)$ relate to the eigenvalues λ_l of $\mathbf{R}$ by

$$\theta_l(h) = \exp(\lambda_l h) \quad \text{or} \quad \lambda_l = \frac{\ln \theta_l(h)}{h} \qquad \forall l = 1, ..., K \tag{29}$$

2. Both $\mathbf{R}$ and $\mathbf{T}(h)$ have identical spectral component matrices $\mathbf{Z}_l$.

As a result, if a Markov chain model is assumed, a transition probability matrix $\mathbf{T}(\Delta h)$ for a discrete lag Δh can be used to compute $\mathbf{R}$ by applying (29) to (26) to obtain

$$\mathbf{R} = \sum_{l=1}^{K} \frac{\ln \theta_l(\Delta h)}{\Delta h} \mathbf{Z}_l \tag{30}$$

where $\theta_l(\Delta h)$ and $\mathbf{Z}_l$ are the eigenvalues and spectral component matrices, respectively, corresponding to $\mathbf{T}(\Delta h)$. Application of (30) to (8) yields

$$\mathbf{T}(h) = \sum_{l=1}^{K} \theta_l(\Delta h)^{h/\Delta h} \mathbf{Z}_l \tag{31}$$

which represents a continuous-lag version of the more commonly used discrete-lag Markov chain model (10). We emphasize that the advantage of (31) over (10) is the continuous functional representation of the model, that is, the ability to calculate $\mathbf{T}(h)$ at any h, not just integer multiples of Δh. Expression (28) shows that a Markov chain model corresponds to a linear combination of exponential functions. Nonetheless, rather nonexponential looking structures can be obtained from a Markov chain model, as evident in some of the off-diagonal transition probabilities for the examples given.

ACKNOWLEDGMENTS

The authors thank J. M. Davis and J. H. Doveton for commentary that substantially improved the paper. This work was supported by Lawrence Livermore National Laboratory, U.S. Geological Survey Water Resources Research Grant 14-18-001-61909, the Monterey Water Resources Agency, U.S. Environmental Protection Agency Grant R819658, Center for Ecological Health Research at University of California at Davis, N.I.E.H.S. Superfund Grant ES-04699, Occidental Chemical Company, University of California Toxic Substances Teaching and Research Program and U.S. Army Corps of Engineers Waterways Experimentation Station. We are also grateful to Lisa Maserjian for collecting and describing cores from the Salinas Valley site and to Karen Burow of the U.S. Geological Survey for providing cores from the Kings River alluvial fan. Although the information in this document has been funded in part by the U.S. Environmental Protection Agency, it does not necessarily

reflect the views of the Agency, and no official endorsement should be inferred.

REFERENCES

AGTERBERG, F. P., 1974, Geomathematics: New York, Elsevier Scientific Publishing Co., 596 p.

ALLEN, J. R. L., 1970, Studies in fluviatile sediments, a comparison of fining-upward cyclothems with special reference to coarse-member composition and interpretation: Journal of Sedimentary Petrology, v. 40, p. 298-323.

ANDERSON, M. P., 1989, Hydrogeologic facies models to delineate large-scale spatial trends in glacial and glaciofluvial sediments: Geological Society of America Bulletin, v. 101, p. 501-511.

ANDERSON, M. P., AND WOESSNER, W. W., 1992, Applied Groundwater Modeling: San Diego, Academic Press Inc., 391 p.

AMERICAN SOCIETY FOR TESTING AND MATERIALS, 1996, Committee D-18 on soil and rock: American Society for Testing and Materials, 257 p.

BIERKENS, M. F. P., 1996, Modeling hydraulic conductivity of a complex confining layer at various spatial scales: Water Resources Research, v. 32, p. 2369-2382.

BLAKE, R. G., NOYES, C. M., AND MALEY, M. P., 1995, Hydrostratigraphic analysis–The key to cost-effective ground water cleanup at Lawrence Livermore National Laboratory: Lawrence Livermore National Laboratory Report UCRL-JC-120614, 13 p.

CARLE, S. F., 1996, A transition probability-based approach to geostatistical characterization of hydrostratigraphic architecture: Unpubl. Ph.D. Dissertation, University of California, Davis, 233 p.

CARLE, S. F., 1997, Implementation schemes for avoiding artifact discontinuities in simulated annealing: Mathematical Geology, v. 29., p. 231-244.

CARLE, S. F., AND FOGG, G. E., 1996, Transition probability-based indicator geostatistics: Mathematical Geology, v. 28, p. 453-476.

CARLE, S. F., AND FOGG, G. E., 1997, Modeling spatial variability with one- and multidimensional continuous-lag Markov chains: Mathematical Geology, v. 29, p. 891-918.

CARR, D. D., HOROWITZ, A., HRARBAR, S. V., RIDGE, K. F., ROONEY, R., STRAW, W. T., WEBB, W., AND POTTER, P. E., 1966, Stratigraphic sections, bedding sequences and random processes: Science, v. 28, p. 89-110.

CASAGRANDE, A., 1948, Classification and identification of soils: Transactions of the American Society of Civil Engineers, v. 113, p. 901-992.

DAVIS, M. J., LOHMANN, R. C., PHILLIPS, F. M., WILSON, J. L., AND LOVE, D. W., 1993, Architecture of the Sierra Ladrones Formation, central New Mexico–Depositional controls on the permeability correlation structure: Geological Society of America Bulletin, v. 105, p. 998-1007.

DEUTSCH, C. V., AND COCKERHAM, P. W., 1994, Practical considerations in the application of simulated annealing in stochastic simulation: Mathematical Geology, v. 26, p. 67-82.

DEUTSCH, C. V., AND JOURNEL, A. G., 1992, GSLIB, Geostatistical Software Library and User's Guide: New York, Oxford University Press, 340 p.

DOMAGALSKI, J. L., AND DUBROVSKY, D. M., 1991, Regional assessment on nonpoint-source pesticide residues in ground water, San Joaquin Valley, California: U.S. Geological Survey Water-Resources Investigations Report 91-4027, 64 p.

DOVETON, J. H., 1971, An application of Markov chain analysis to the Ayrshire Coal Measures succession: Scottish Journal of Geology, v. 7, p. 11-27.

DOVETON, J. H., 1994, Theory and applications of vertical variability measures from Markov chain analysis, *in* Yarus, J. M., and R. L. Chambers eds., Stochastic Modeling and Geostatistics–Principles, Methods, and Case Studies: American Association of Petroleum Geologists Computer Applications in Geology, no. 3, p. 55-64.

DURHAM, D. L., 1974, Geology of the southern Salinas Valley area, California: U.S. Geological Survey Professional Paper 819, 111 p.

ETHERIDGE, F. G., AND SCHUMM, S. A., 1978, Reconstructing paleochannel morphologic and flow characteristics–Methodology, limitations, and assessment, *in* Miall, A. D., ed., Fluvial Sedimentology: Canadian Society of Petroleum Geologists Memoir 5, p. 703-721.

FOGG, G. E., 1989, Emergence of geologic and stochastic approaches for characterization of heterogeneous aquifers, *in* Proceedings, New Field Techniques for Quantifying the Physical and Chemical Properties of Heterogeneous Aquifers, Dallas, Texas, March 20-23, 1989: National Water Well Association, Dublin, Ohio, p. 1-17.

FOGG, G. E., ROLSTON, D. E., LABOLLE, E. M., BUROW, K. R., MASERJIAN, L. A., DECKER, D. A., AND CARLE, S. F., 1995, Matrix diffusion and contaminant transport in granular geologic materials, with case study of nitrate contamination in Salinas Valley, California: Final Technical Report submitted to Monterey County Water Research Agency and U.S. Geological Survey under Water Resources Research Award No. 14-08-0001-G1909, 65 p. and appendices.

GOMEZ-HERNANDEZ, J. J., AND SRIVASTAVA, R. M., 1990, ISIM3D, an ANSI-C three-dimensional multiple indicator conditional simulation program: Computers and Geosciences, v. 16, p. 395-440.

HARBAUGH, J. W., AND BONHAM-CARTER, G. F., 1970, Computer Simulation in Geology: New York, Wiley Interscience, 575 p.

HATTORI, I., 1976, Entropy in Markov chains and discrimination of cyclic patterns in lithologic successions: Mathematical Geology, v. 8, p. 477-497.

HUNTINGTON, G.L., 1980, Soil-land form relationships of portions of the San Joaquin River and Kings River alluvial depositional systems in the Great Valley of California: Unpubl. Ph.D. Dissertation, University of California, Davis, 147 p.

JOHNSON, N. M., 1995, Characterization of alluvial hydrostratigraphy with indicator semivariograms: Water Resources Research, v. 31, p. 3205-3216.

JOHNSON, N. M., AND DREISS, S. J., 1989, Hydrostratigraphic interpretation using indicator geostatistics: Water Resources Research, v. 25, p. 2501-2510.

JOURNEL, A. G., AND ALABERT, F., 1990; New method for reservoir mapping: Journal of Petroleum Technology, v. 42, p. 212-218.

KLOOS, H., 1983, DBCP pesticide in drinking water wells in Fresno and other communities in the Central Valley of California: Ecology of Disease, v. 2, p. 363-367.

KOLTERMANN, C. E., AND GORELICK, S. M., 1992, Paleoclimatic signature in terrestical flood deposits: Science, v. 256, p. 1775-1782.

KRUMBEIN, W. C., 1968, Fortran IV computer program for simulation of transgression and regression with continuous-time Markov models: Computer Contribution 26, Kansas State Geological Survey, 38 p.

KRUMBEIN, W. C., AND DACEY, M. F., 1969, Markov chains and embedded Markov chains in geology: Mathematical Geology, v. 1, p. 79-96.

LEEDER, M. R., 1982, Sedimentology: London, George Allen & Unwin, 344 p.

LIN, C., AND HARBAUGH, J. W., 1984, Graphic Display of Two- and Three- Dimensional Markov Computer Models in Geology: New York, Van Nostrand Reinhold, 180 p.

MASERJIAN, L. A., 1993, Hydrogeologic analysis of the unsaturated zone, northern Salinas Valley, California: Unpubl. M.S. Thesis, University of California, Davis, p.

MIALL, A. D., 1973, Markov chain analysis applied to an ancient alluvial plain succession: Sedimentology, v. 20, p. 347-365.

MIALL, A. D., 1982, Analysis of fluvial depositional systems: American Association of Petroleum Geologists, Education course note series # 20, 75 p.

MIALL, A. D., 1992, Alluvial deposits, *in* Walker, R. C., and James, N. P., eds., Facies Models: Geological Association of Canada, p. 119-142.

NETON, M. J., DORSCH, J., OLSON, C. D., AND YOUNG, S. C., 1994, Architecture and directional scales of heterogeneity in alluvial fan aquifers: Journal of Sedimentary Research, v. B64, p. 245-247.

NIGHTINGALE, H. I., 1970, Statistical evaluation of salinity and nitrate content and trends beneath urban and agricultural areas - Fresno, California: Ground Water, v. 8, p. 22-28.

NOYES, C. N., 1991, Hydrostratigraphic analysis of the Pilot Remediation Test Area, LLNL, Livermore, California: Unpubl. M.S. Thesis, University of California, Davis, 165 p.

PHILLIPS, F. M., AND WILSON, J. L., 1989, An approach to estimating hydraulic conductivity spatial correlation scales using geologic characteristics: Water Resources Research, v. 25, p. 141-143.

POETER, E. P., AND MCKENNA, S. A., 1995, Reducing uncertainty associated with ground-water flow and transport predictions: Ground Water, v. 33, p. 899-904.

POLITIS, D. N., 1994, Markov chains in many dimensions: Advances in Applied Probability, v. 26, p. 756-774.

PRESS, W. H., TEUKOLSKY, S. A., VETTERLING, W. T., AND FLANNERY, B. P., 1992, Numerical Recipes in Fortran: New York, Cambridge University Press, 963 p.

QUALHEIM, B. J., 1988, Well log report for the LLNL ground water project 1984-1987: Lawrence Livermore National Laboratory Report UCID-21342 (updated 1989, 1993), 12 p. and 304 oversize sheets.

RITZI, R. W., DOMINIC, D. F., BROWN, N. R., KAUSCH, K. W., MCALENNEY, P. J., AND BASIAL, M. J., 1995, Hydrofacies distribution and correlation in the Miami Valley aquifer system: Water Resources Research, v. 31, p. 3271-3281.

RITZI, R. W., JAYNE, D. F., ZAHRADNIK, A. J., FIELD, A. A., AND FOGG, G. E.,, 1994, Geostatistical modeling of heterogeneity in glaciofluvial, buried-valley aquifers: Ground Water, v. 32, p. 666-674.

ROSS, S., 1993, Introduction to Probability Models, 5th ed.: San Diego, Academic Press, 556 p.

SCHEIBE, T. D., AND FREYBERG, D. L., 1995, Use of sedimentological information for geometric simulation of natural porous media structure: Water Resources Research, v. 31., p. 3259-3270.

SCHWARZACHER, W., 1969, The use of Markov chains in the study of sedimentary cycles: Mathematical Geology, v. 12, p. 213-234.

SMITH, B. T., BOYLE, J. M., DONGARRA, J. J., GARBOW, B. S., IKEBE, Y., KLEMA, V. C., AND MOLER, C. B., 1976, Matrix eigensystem routines–EISPACK guide, *in* Lecture Notes in Computer Science, 2d ed.: New York, Springer-Verlag, v. 6, 551 p.

SURO-PEREZ, V., AND JOURNEL, A. G., 1991, Indicator principal component kriging: Mathematical Geology, v. 23, p. 759-788.

SWITZER, P., 1965, A random set process in the plane with a Markovian property (note): Annals of Mathematical Statistics, v. 36, p. 1859-1863.

TETZLAFF, D. M., AND HARBAUGH, J. W., 1989, Simulating Clastic Sedimentation: New York, Van Nostrand Reinhold, 202 p.

THORPE, R. K., ISHERWOOD, W. F., DRESEN, M. D., AND WEBSTER-SCHOLTEN, C. 1990, CERCLA Remedial Investigations Report for the LLNL Livermore site: Lawrence Livermore National Laboratory Report UCAR-10299.

TINSLEY, J. C., III, 1975, Quaternary geology of the northern Salinas Valley, Monterey County, California: Unpubl. Ph.D. Dissertation, Stanford University, Stanford, California, 201 p.

TURK, G., 1979, Transition analysis of structural sequences– Discussion: Geological Society of Americal Bulletin, v. 90, p. 989-991.

TURK, G., 1982, Markov chains–Letters to the Editor: Mathematical Geology, v. 14, p. 539-542.

U.S. DEPARTMENT OF AGRICULTURE, 1971, Soil survey, eastern Fresno area, California: U.S. Department of Agriculture Soil Conservation Service, Washington, D.C., 323 p.

VISTELIUS, A. B., 1949, On the question of the mechanism of formation of strata: Doklady Akademii Nauk, SSSR, v. 65, p. 191-194.

VISTELIUS, A. B., 1967, Studies in Mathematical Geology: New York, Consultants Bureau, p. 252-258.

WEBB, E. K., AND ANDERSON, M. P., 1996, Simulation of preferential flow in three-dimensional heterogeneous conductivity fields with realistic internal architecture: Water Resources Research, v. 32, p. 533-545.

WEN, X. H., AND KUNG, C. S., 1993, Stochastic simulation of solute transport in heterogeneous formations–A comparison of parametric and nonparametric geostatistical approaches: Ground Water, v. 31, p. 953-965.

WINGLE, W. L., AND POETER, E. P., 1993, Uncertainty associated with semivariograms used for site simulation: Ground Water, v. 31, p. 725-734.